



HAL
open science

Attenuation, source parameters and site effects in the Irpinia-Basilicata region (southern Apennines, Italy)

Luciana Cantore, Adrien Oth, Stefano Parolai, Dino Bindi

► **To cite this version:**

Luciana Cantore, Adrien Oth, Stefano Parolai, Dino Bindi. Attenuation, source parameters and site effects in the Irpinia-Basilicata region (southern Apennines, Italy). *Journal of Seismology*, 2011, 15 (2), pp.375-389. 10.1007/s10950-011-9230-2 . hal-00670741

HAL Id: hal-00670741

<https://hal.science/hal-00670741>

Submitted on 16 Feb 2012

HAL is a multi-disciplinary open access archive for the deposit and dissemination of scientific research documents, whether they are published or not. The documents may come from teaching and research institutions in France or abroad, or from public or private research centers.

L'archive ouverte pluridisciplinaire **HAL**, est destinée au dépôt et à la diffusion de documents scientifiques de niveau recherche, publiés ou non, émanant des établissements d'enseignement et de recherche français ou étrangers, des laboratoires publics ou privés.

Attenuation, source parameters and site effects in the Irpinia-Basilicata region (southern Apennines, Italy)

Luciana Cantore¹, Adrien Oth^{2,*}, Stefano Parolai³, Dino Bindi⁴

- 1) Dipartimento di Scienze Fisiche, Università degli Studi di Napoli Federico II, Naples I-80125, Italy.
- 2) European Center for Geodynamics and Seismology, rue Josy Welter 19, L-7256 Walferdange, Luxembourg
- 3) Helmholtz Centre Potsdam, GFZ German Research Centre for Geosciences, Earthquake Risk and Early Warning Section, Telegrafenberg, D-14473 Potsdam, Germany
- 4) Helmholtz Centre Potsdam, GFZ German Research Centre for Geosciences, Centre for Disaster Management and Risk Reduction Technology (CEDIM), Telegrafenberg, D-14473 Potsdam, Germany

*Corresponding author, adrien.oth@ecgs.lu

ABSTRACT

We derive S-wave attenuation characteristics, earthquake source parameters and site amplification functions at seismic stations used for earthquake early warning in the Irpinia-Basilicata region, using non-parametric spectral inversion of seismograms from 49 local events with $M_L=1.5-3.1$. We obtain relatively low Q-values ($Q_0=28$ at a frequency of 1 Hz) in conjunction with a strong frequency-dependence (close to linear). The source spectra can be satisfactorily modeled using the omega-square model, with stress drops ranging between 0.01-2 MPa, and in the narrow magnitude range available for analysis, the source spectra seem to scale self-similarly. The local magnitude M_L shows a linear correlation with moment magnitude M_W , however with a systematic underestimation by about 0.5 magnitude units. The results obtained in this work provide important insights into the ground motion characteristics that are required for appropriate seismic hazard assessment and are of practical relevance for a suite of applications, such as the calibration of ground-motion prediction equations or the correction for site amplification in earthquake early warning and rapid calculation of shake-maps for seismic emergency management.

INTRODUCTION

1
2
3 The southern Apennines represent an active tectonic region within Italy that
4
5 accommodates differential motions between the Adria and Tyrrhenian microplates,
6
7 responsible for almost all of the seismicity occurring in this region. Recent in situ stress
8
9 data research (Montone et al., 2004) and seismological data analysis indicate that an
10
11 extensional stress regime is prevalent in the southern Apennines, and that the seismic
12
13 activity is confined to the narrow upper-crustal seismic zone. In particular, two main
14
15 clusters of crustal earthquakes may be identified: the westernmost cluster with shallow
16
17 earthquakes (depths < 20 km) along the axis chain (Irpinia area) and the easternmost cluster
18
19 with deeper earthquakes (about 20-40 km) located on the outer margin of the chain
20
21 (Potentino area) and the foredeep. The earthquakes in these two clusters show different
22
23 focal mechanisms indicating a pure extensional regime to the west (Irpinia) and a strike-slip
24
25 regime to the east (Potentino).
26
27
28
29
30
31

32
33 During the last century, three large earthquakes with magnitudes greater than 6 have
34
35 occurred in the Irpinia-Basilicata region: the 1930 M 6.7 Irpinia earthquake (Emolo et al.,
36
37 2004), the 1962 M 6.2 Irpinia earthquake (Westaway, 1987), and the 1980 M 6.9 Irpinia-
38
39 Basilicata earthquake (Westaway and Jackson, 1987; Bernard and Zollo, 1989; Pantosti and
40
41 Valensise, 1990). Particularly the 1980 Irpinia-Basilicata earthquake caused catastrophic
42
43 damage throughout the region, resulting in about 3,000 fatalities. Today, seismicity is
44
45 mainly concentrated within or close to the fault system associated with the 1980 Irpinia-
46
47 Basilicata earthquake and several moderate-size events occurred in recent years, such as the
48
49 1990 and 1991 Potenza earthquakes (M 5.4 and 5.1, within the deeper strike-slip zone) and
50
51 the 1996 event (M 4.9). This recent seismic activity provides clear indications that the
52
53 Irpinia-Basilicata region still represents a region of high seismic risk, now and in the future
54
55 (Cinti et al., 2004).
56
57
58
59
60
61
62
63
64
65

1
2
3 In response to this threat, an earthquake early warning system prototype is in
4
5 development in the Campania-Lucania region, the core of which is made up of the dense
6
7 Irpinia Seismic Network (ISNet) recently installed along the southern Apennines chain
8
9 (Figure 1). It is equipped with sensors that can provide high-quality recordings of both
10
11 weak motions from small-magnitude events as well as strong ground shaking, thus enabling
12
13 scientists to retrieve information about the rupture processes and to obtain insights into the
14
15 scaling relationships between small and large events (Convertito et al., 2009). The network
16
17 consists of 27 seismic instruments and covers an area of approximately 100x70 km² and
18
19 has been especially designed to provide optimal coverage of the active fault system that
20
21 generated the November 23 1980 Irpinia earthquake (Weber et al., 2007). Each station is
22
23 equipped with a strong-motion accelerometer (Guralp CMG-5T) and a short period three-
24
25 component seismometer (Geotech S13-J with natural period of 1 second), thus covering the
26
27 entire necessitated dynamic recording range.
28
29
30
31
32
33
34

35 The ISNet seismic network was installed with the purpose of monitoring in real-time
36
37 the potential source region of destructive earthquakes (i.e., the region around the source
38
39 zone of the 1980 event) that, beyond the evident threat that these pose within the immediate
40
41 source area, also represent a serious danger to the city of Naples and the densely populated
42
43 coast. Thus, it is of utmost importance to provide the best possible characterization of the
44
45 seismic recordings obtained at this local-scale network. One major aim of the work
46
47 presented in this article is therefore to characterize the frequency-dependent site response
48
49 for the ISNet stations by applying the generalized inversion technique (GIT) to the Fourier
50
51 amplitude spectra (FAS) of ground motion. In addition to the information on site response,
52
53 this technique provides us with insights into seismic attenuation characteristics within the
54
55 area covered by the network as well as source spectra of the utilized events, parameters that
56
57
58
59
60
61
62
63
64
65

1
2
3 are of considerable importance to better understand seismic ground motions in the area.
4

5
6 We first provide an overview of the dataset and the applied methodology, followed by
7
8 a discussion of seismic attenuation and, in particular, its frequency-dependence. From the
9
10 source spectra, we investigate the scaling characteristics in the available magnitude range,
11
12 derive the stress drops of the events and discuss the scaling relation between local and
13
14 moment magnitude. Finally, the site response functions for the ISNet stations are discussed
15
16 and compared to the H/V spectral ratios calculated directly from the ground motion spectra.
17
18
19

20 21 **DATASET**

22
23 Seismograms from 49 local earthquakes that occurred between February 2006 and
24
25 November 2008 recorded by the short-period sensors of 22 ISNet stations constitute the
26
27 basis of our analysis. Data were recorded with a sampling rate of 125 samples per second,
28
29 and we only considered events and stations with at least 3 available recordings. For most
30
31 earthquakes and stations, however, more than 5 respectively 10 records could be used.
32
33 Figure 2 shows the station locations, the epicenters of the selected events and the source-
34
35 station travel paths, which together show a satisfactory coverage of the area inside the
36
37 network. The hypocentral distances range from 5 to 83 km with best coverage between 10
38
39 to 65 km (Figure 3a), and the focal depths of the events are all shallower than 30 km. The
40
41 covered magnitude range is rather narrow ($1.5 < M_L < 3.1$) (Figure 3b), with the largest
42
43 number of events in the range $M_L = 1.5 - 2.5$.
44
45
46
47
48
49

50
51 The records were baseline corrected, the effect of instrumental response was removed
52
53 and the resulting seismograms were finally high-pass filtered applying a four-pole
54
55 Butterworth filter with corner frequency 0.2 Hz. For the purpose of our analysis, only the S-
56
57 wave portions of the records were used. Time windows starting 1 sec before the S-wave
58
59 onset (picked on the horizontal components) with a length of 5 sec were extracted. Before
60
61
62
63
64
65

1
2
3 calculation of the FAS, the beginning and end of each window were tapered with a 5%
4
5 cosine window and the computed spectra were smoothed around 40 frequency points
6
7 equally spaced on logarithmic scale between 1 and 30 Hz using the smoothing function
8
9 proposed by Konno and Ohmachi (1998) with $b = 40$. Pre-event noise windows with the
10
11 same length as the S-wave windows were used to compute the signal-to-noise (SNR) ratio
12
13 and at each frequency point, only records with a SNR higher than 3 were considered. Due
14
15 to this SNR-based selection, the number of data points entering the inversion is slightly
16
17 different at each frequency. Finally, the horizontal- component spectra were combined to
18
19 their root-mean-square (rms) average.
20
21
22
23
24

25 **METHODS**

26
27 In order to separate source spectra, attenuation characteristics and site response
28
29 functions from one another, we applied a two-step non-parametric spectral inversion
30
31 scheme as originally proposed by Castro et al. (1990) (termed below as generalized
32
33 inversion technique, GIT) to the velocity spectra of the ISNet S-wave records. We applied
34
35 the GIT inversion both to horizontal and vertical components and compared the site
36
37 response functions obtained by the GIT inversion with the H/V ratios calculated directly
38
39 from the observed ground motion spectra at each station.
40
41
42
43
44

45 **Generalized inversion technique (GIT)**

46
47 Since the applied GIT approach is commonly used in the literature (e.g. Castro et al.,
48
49 1990; Parolai et al., 2000, 2004; Oth et al., 2008, 2009), we limit our discussion on the
50
51 methodology to the basic concept and refer the reader to the latter publications for the
52
53 details. We followed the two-step procedure introduced by Castro et al. (1990): in the first
54
55 step, the dependence of the spectral amplitudes on distance for a given frequency f is given
56
57
58
59
60 by
61
62
63
64
65

$$U_{ij}(f, r_{ij}) = A(f, r_{ij}) \cdot \hat{S}_j(f), \quad (1)$$

where $U_{ij}(f, r_{ij})$ represents the observed spectral amplitude at the i -th station resulting from the j -th earthquake, r_{ij} is the source-site distance, $A(f, r_{ij})$ is the non-parametric attenuation function, and $\hat{S}_j(f)$ is a scalar factor that depends on the size of the j -th source. In this model, the functional form of $A(f, r_{ij})$ is not pre-defined and implicitly includes all effects causing attenuation along the travel path (geometrical spreading, anelasticity, scattering, etc.). Since the properties causing attenuation within the Earth's crust are thought to vary slowly with distance, $A(f, r_{ij})$ is constrained to be a smooth decaying function with distance r and to take the value $A(f, R_0) = 1$ at a specific reference distance R_0 (5 km in our case). Site effects are not included in the formulation given by equation (1) and are supposed to be primarily absorbed into the residuals of the observed ground motion spectra from this parameterization.

For N spectral records, equation (1) represents a linear system of N equations, which is formed for each frequency analyzed by taking the logarithm. The system of equations is solved using singular value decomposition (Menke, 1989), providing us with discretized (in bins of 2 km) attenuation functions $A(f, r_{ij})$ and the source scaling factors.

Estimates of the quality factor can be obtained through fitting a parametric model to $A(f, r)$:

$$A(f, r) = G(r) \exp\left(-\frac{\pi f r}{Q(f) v_s}\right). \quad (2)$$

Herein, $Q(f)$ is the S-wave quality factor, v_s the average shear wave velocity and $G(r)$ represents the geometrical spreading function. Since at distances larger than 70 km the attenuation functions are only constrained by very few data points, we only used the

1
2
3 attenuation functions within distances lower than 70 km to derive $Q(f)$, setting the
4
5 geometrical spreading function to $G(r)=5/r$. From equation (2), $Q(f)$ can be evaluated from
6
7 the slope of a linear least-squares fit to $\log A(f,r)-\log G(r)$ versus distance. Finally, we
8
9 investigate the frequency dependence of Q assuming a model of the form $Q(f) = Q_0 f^N$.

10
11
12
13
14 After the attenuation functions $A(f, r_{ij})$ have been determined, the spectral amplitudes
15
16 at each frequency are corrected for the effect of seismic attenuation and in the second
17
18 inversion step, the corrected spectra are separated into source and site effects (Andrews,
19
20 1986):

$$21 \quad R_{ij}(f) = S_j(f) \cdot Z_i(f) \quad (3)$$

22
23
24 Here, $R_{ij}(f) = U_{ij}(f, r_{ij})/A(f, r_{ij})$ are the residual spectral amplitudes after correction
25
26 for path effects, $S_j(f)$ is the source spectrum of the j-th earthquake, and $Z_i(f)$ the site
27
28 amplification function at the i-th station. Equation (3) can be linearized as well by applying
29
30 the logarithm.

31
32
33 As noted by Andrews (1986), equation (3) still contains one undetermined degree of
34
35 freedom due to the linear dependence between site and source terms. This degree of
36
37 freedom must be fixed by setting a reference condition either for at least one source or one
38
39 site in the dataset. Usually, the site response of a rock site is fixed to one (respectively zero
40
41 in \log_{10}), irrespective of frequency, or the average site response at a set of competent sites is
42
43 set to unity.

44
45
46 We solved the second inversion by constraining the logarithm of the site
47
48 amplification of a reference site to zero. We adopted station AND3 as the reference site
49
50 because it is located on outcropping bedrock and the H/V ratio at this station is flat and
51
52 almost equal to one over the entire analyzed frequency range (Figure 4), except at the
53
54
55
56
57
58
59
60
61
62
63
64
65

1
2
3 lowest frequencies where there is a slight increase to a factor of about two. In order to
4
5 evaluate the stability of the solution and estimate standard errors for the model parameters,
6
7 we performed 200 bootstrap inversions (Efron and Tibshirani, 1994) for each of the 40
8
9 frequency points following the same procedure as used by Parolai et al. (2000, 2004) and
10
11 Oth et al. (2008, 2009). From the 200 bootstrap samples, the mean and standard error were
12
13 calculated for each model parameter.
14
15

16 17 18 **H/V ratios of earthquake data** 19

20
21 The GIT site responses have been compared with those calculated by horizontal-to-
22
23 vertical (H/V) ratios derived from earthquake data. The H/V method, originally introduced
24
25 by Nakamura (1989) to interpret microtremor recordings, has become a very popular tool in
26
27 site response estimation in recent years. Lermo and Chavez-Garcia (1993) first applied this
28
29 technique to the S-wave part of earthquake recordings as well. The H/V method, in analogy
30
31 to the so-called receiver-function technique used to investigate the crustal and upper mantle
32
33 structures from teleseismic records (Langston, 1979), assumes that the vertical component
34
35 of ground motion is mainly controlled by source and attenuation effects and is not very
36
37 sensitive to local site amplification. Thus, by deconvolving, or dividing in the frequency
38
39 domain, the vertical component from the horizontal one, an estimate of the site response
40
41 function can be obtained. Because the S-wave amplification at the surface depends on the
42
43 angle of incidence (Lermo and Chavez-Garcia, 1993), it is necessary to average over a
44
45 sufficient number of events distributed around the station of interest with good azimuthal
46
47 and distance coverage in order to obtain stable estimates (Parolai et al., 2004).
48
49
50
51
52
53

54
55 Generally, comparisons of site response functions obtained with different techniques
56
57 (e.g., Field and Jacob, 1995; Bonilla et al., 1997; Parolai et al., 2004) have shown that the
58
59 H/V method provides a good estimate of the fundamental frequency of resonance, but
60
61
62
63
64
65

1
2
3 underestimates the level of amplification with respect to the GIT. Recently, Parolai and
4
5 Richwalski (2004) showed that the observed differences in the estimated amplifications
6
7 obtained applying different techniques could be linked to S-P conversions at the bottom of
8
9 the soft layer in the case of high impedance contrasts.
10

11 12 13 **RESULTS**

14 15 **Attenuation characteristics**

16
17
18 The obtained non-parametric attenuation functions at all 40 frequency points are
19
20 depicted in Figure 5a, color-coded with respect to their frequency, while in Figure 5b, two
21
22 of the attenuation curves are depicted together with their estimated standard deviation from
23
24 the bootstrap analysis. The latter plot shows that in general the attenuation curves are well
25
26 constrained. The functions depict a relatively simple shape, being all monotonically
27
28 decaying with a change in the rate of amplitude decay for hypocentral distances between 20
29
30 and 50 km at higher frequencies. Below 20 km distance, the high frequencies show a
31
32 stronger decay with distance, while between 20 and 50 km, the slope of the attenuation
33
34 curves adjusts to be very similar for almost the entire frequency band.
35
36
37
38
39
40

41 Figure 6 shows the values of $Q(f)$ estimated for all frequencies using equation (2) (the
42
43 vertical error bars indicate the regressional error of fit) and the least-squares fit of a relation
44
45 of the form $Q(f) = Q_0 f^N$ obtained with these values (solid black line). As can be seen from
46
47 Figure 6, the frequency-dependence of $Q(f)$ can be well approximated with a power-law
48
49 dependency given as:
50
51
52

$$53 \quad Q(f) = 28.3 f^{0.87} \quad (4)$$

54
55 We thus find a rather strong frequency-dependence of the quality factor in the region.
56
57
58 Other models derived for different regions in Italy, including southern Italy where the
59
60
61
62

1
2
3 region under investigation by this study is located, are indicated in Figure 6 as well (within
4
5 the overlap of the frequency range of their validity and the range 1-30 Hz of our study, see
6
7 also Table 1). In particular, Castro et al. (2004b) derived the relationship $Q(f) = 32.1f^{1.7}$
8
9 from a dataset of 32 earthquakes recorded at 4 stations of the Basilicata seismic network.
10
11 They obtained a much stronger frequency-dependence with $N>1$, while in contrast the
12
13 value of Q_0 is rather close to the one found here. Castro et al. (2008) corroborated the
14
15 results of Castro et al. (2004b), using a significantly extended dataset from the same
16
17 seismic network. They furthermore used a more sophisticated analysis procedure on their
18
19 non-parametric attenuation curves, providing separate estimations of upper and lower
20
21 crustal attenuation characteristics in the frequency range 1-25 Hz. Assuming body-wave
22
23 geometrical spreading ($\propto 1/r$) over the first 50 km, they obtained the Q-model
24
25 $Q(f) = 18.8f^{1.7}$ for the upper crust (depth < 13 km). While this frequency dependence is
26
27 identical to one obtained by Castro et al. (2004b), attenuation is slightly larger at all
28
29 frequencies due to the lower Q_0 value (18.8 vs. 32.1). Considering however the typical
30
31 uncertainty ranges in determining such Q(f) models, the results of both studies are highly
32
33 consistent with one another, and we only list the result of Castro et al. (2004b) in Table 1
34
35 and Figure 6. Another study covering the region of interest investigated coda-Q in the
36
37 frequency range 1-12 Hz (Bianco et al., 2002) and the authors found from a multi lapse
38
39 time window analysis that intrinsic Q seems to dominate with respect to scattering Q in the
40
41 area. Other Q-models have been reported for different regions of Italy by Rovelli et al.
42
43 (1988), Malagnini et al. (2000) and Castro et al. (2004a,b), and the one that matches our
44
45 results most closely is the model for Umbria given by Castro et al. (2004a), with a
46
47 frequency-dependence $N=1.2$. It is important to point out that due to the trade-off between
48
49 Q and the geometrical spreading function, a reliable comparison between the different
50
51
52
53
54
55
56
57
58
59
60
61
62
63
64
65

1
2
3 models only makes sense if the estimates of Q are made using similar geometrical
4
5 spreading functions. Moreover, it should be noted that the data used to retrieve the
6
7 attenuation models listed in Table 1 sample different frequency bands and different crustal
8
9 volumes. The studies by Malagnini et al. (2000) and Rovelli et al. (1988) sample for
10
11 instance large regions such as the entire Apennines or the entirety of southern Italy. In
12
13 contrast, our results are related to a small area limited by the extent of the ISNet network,
14
15 and also Bianco et al. (2002) analyzed data from a much larger area surrounding the ISNet
16
17 network. This limitation of our study to the small region covered by the ISNet network can
18
19 however also be seen as an advantage in the sense that with the derived attenuation
20
21 functions, we provide a means for reliable and consistent attenuation correction for events
22
23 occurring in close proximity or within the network, avoiding a bias in source parameter or
24
25 site response estimation due to inappropriate attenuation correction.
26
27
28
29
30
31

32 **Source spectra**

33
34
35 In order to remove the undetermined degree of freedom when separating source
36
37 spectra and sites response from the attenuation-corrected spectral amplitudes as described
38
39 by equation (3), we fixed the site response at the reference station AND3 to unity,
40
41 irrespective of frequency. Since with the non-parametric attenuation functions discussed
42
43 above we can only correct for attenuation up the reference distance of 5 km (i.e. the lowest
44
45 distance in our dataset), the obtained source spectra from the second inversion step are also
46
47 given at the reference distance of 5 km.
48
49
50
51
52

53 We did not include a term accounting for potential high-frequency decay due to the
54
55 exponential κ -operator (Anderson and Hough, 1984) in the reference condition, and it may
56
57 therefore be the case that some high-frequency decay due to near-surface high-frequency
58
59 diminution at the reference site is systematically shifted into the source spectra. In order to
60
61
62
63
64
65

investigate this issue, we plot the source spectra in acceleration (Figure 7a) and visually checked the high-frequency part of the spectra. As can be seen from Figure 7a, the acceleration source spectra generally show a clear plateau-like structure at highest frequencies, as would be expected in the case the ω^2 -model (Brune, 1970, 1971) is valid. Thus we cannot see any clear indication that a systematic high-frequency decay is moved into the source contributions. There is one systematic through appearing in the source spectra at a frequency of about 22-23 Hz, which may be due to an amplification effect at the reference station not accounted for in the inversion constraint.

In order to derive the source parameters (i.e. seismic moments and corner frequencies) of the 49 earthquakes in our dataset, we fitted the ω^2 -model to the inverted source spectra (in acceleration, using the results from the horizontal component inversion) using non-linear least squares:

$$S(f) = (2\rho f)^2 \cdot \frac{R^{0\phi} VF}{4\rho r v_s^3 R_0} \cdot M_0 \cdot \left[1 + \frac{f^2}{f_C^2} \right]^{-1}, \quad (5)$$

where $R^{0\phi}$ is the average radiation pattern set to 0.55, $V=1/\sqrt{2}$ accounts for the separation of S-wave energy on two horizontal components, $F=2$ is the free surface amplification, $\rho=2.8 \text{ g/cm}^3$ is the density, and $v_s = 3.3 \text{ km/sec}$ is the estimated average shear-wave velocity in the source region. $R_0=5 \text{ km}$ represents the reference distance, M_0 denotes the seismic moment, and f_C is the corner frequency. Finally, we compute stress drop estimates from the moment and corner frequencies following Hanks and Thatcher (1972):

$$DS = 8.5 \cdot M_0 \cdot \left(\frac{f_C}{v_s} \right)^3. \quad (6)$$

1
2
3 The ω^2 fits to the inverted source spectra are indicated in Figure 7a as dashed green
4
5 lines, showing that the source spectra can satisfactorily be explained using the ω^2 -model.
6
7 Figure 7b shows corner frequency plotted versus seismic moment (on a log-log scale), with
8
9 the regressional errors of fit (obtained when fitting equation (5) to the source spectra)
10
11 indicated as horizontal respectively vertical error bars. In the case of self-similar scaling,
12
13 the relationship $M_0 \propto f_c^{-3}$ holds and the slope of a fitted straight line in Figure 7b should
14
15 be close to -1/3. Indeed, we note that this is approximately the case, but at the same time, it
16
17 is clear that the magnitude range under investigation in this article is much too small to
18
19 draw any general conclusions on this issue. The stress drops derived using equation (6)
20
21 range between 0.01 and 2 MPa (Figure 7c). While this is still within the bounds generally
22
23 found for crustal earthquakes (~0.1-100 MPa, e.g. Kanamori, 1994), the values clearly
24
25 range at the bottom of this range, indicating comparatively low stress drops for the small
26
27 earthquakes in this area. Since earthquakes with low stress drops radiate only little high-
28
29 frequency energy as compared with high stress drop events, this observation can also
30
31 explain the fact that the local magnitude M_L generally underestimates the moment
32
33 magnitude M_W by about 0.5 magnitude units, but is otherwise approximately linearly
34
35 correlated with the latter (Figure 7d).
36
37
38
39
40
41
42
43
44

45 **Site response**

46
47
48 Based on the local geological conditions, the stations were divided into three groups,
49
50 depending on whether they are located on alluvial deposits, debris or colluvial deposits,
51
52 respectively rock. The geologic characteristics of the sites correspond to the following
53
54 approximate classification: soft soil, stiff soil and rock (Table 2). The GIT horizontal
55
56 component site response functions are shown in Figure 8 for six exemplary stations, with
57
58 two stations from each group. As mentioned earlier, station AND3 (not shown in Figure 7)
59
60
61
62
63
64
65

1
2
3 was chosen as the reference site, assuming a site response of unity, irrespective of
4
5 frequency, since this station is classified as a hard rock site and the H/V ratio is roughly flat
6
7 and approximately equal to one over the entire analyzed frequency band (Figure 4).
8
9

10
11 Figure 8 shows that in general the obtained site response functions are well
12
13 constrained, with only small standard deviations resulting from the bootstrap analysis.
14
15 Overall, the rock sites show as expected lower values of the site response functions over the
16
17 entire frequency band than stiff and soft soil sites, with no evident predominant frequency
18
19 peaks. However, it can be clearly seen that also stations located on rock outcrops are not
20
21 completely devoid of amplification effects (e.g. station VDS3), which may be linked to the
22
23 weathered and fractured nature of the surface layers and to the shear-wave velocity gradient
24
25 (e.g. Theodulidis and Bard, 1995; Steidl et al., 1996). On the other hand, stations classified
26
27 as soft soil and stiff soil generally show more prominent amplification effects, with
28
29 amplification peaks at some given distinct frequencies (e.g. 4-5 Hz at station CLT3, 8 Hz at
30
31 station PGN3). The most significant amplification effects were obtained at station CMP3,
32
33 attaining a factor of about 14 at frequencies of about 8 and 12 Hz.
34
35
36
37
38
39

40
41 We also carried out a GIT inversion for the vertical (Z) component using the same S-
42
43 wave windows as chosen for the horizontal (H) one, and in order to corroborate the site
44
45 amplification functions obtained from the inversion, we calculated the H/V ratios directly
46
47 from the observed ground motion spectra as well. For the Z component GIT inversion, we
48
49 used the same reference condition as for the H component, i.e. the site response at station
50
51 AND3 is set to unity, irrespective of frequency.
52
53
54

55
56 Figure 9 shows the comparison of the GIT H/Z ratio (i.e. the horizontal-to-vertical
57
58 ratio of the GIT site response functions, solid black line) and the H/V ratios (solid black
59
60 line with circles) for the same six stations as depicted in Figure 8. The individual GIT site
61
62
63
64
65

1
2
3 amplification functions for the H (same as shown in Figure 8) and Z components are
4 indicated as well (grey lines with inverted triangles and squares, respectively). A first
5 observation is that the GIT H/Z ratio can satisfactorily explain the main features observed
6 in the H/V ratios (see for instance the peak at 4-5 Hz for station CLT3), with some
7 discrepancies only at low frequencies. These discrepancies may be linked to the fact that,
8 due to the reference condition, the GIT H/Z ratio at station AND3 is equal to unity, while at
9 the lowest frequencies, the H/V ratio observed at station AND3 starts to rise to about a
10 factor of two. Therefore, it is expectable that the GIT H/Z ratios slightly underestimate the
11 H/V ratios at low frequencies.
12
13
14
15
16
17
18
19
20
21
22
23
24

25 Another striking observation is given by the fact that the GIT site response function
26 of the Z component shows remarkable amplification effects for some stations (e.g. CMP3),
27 with the maximum of amplification shifted to higher frequencies as compared with the H
28 component. In such cases, the H/V ratio shows significant differences with the GIT H
29 amplification function, and as Parolai and Richwalski (2004) showed, this effect can be
30 linked to S-P conversions at the bottom of the soft layer in the case of high-impedance
31 contrasts, leading to a reduction of the H/V amplitude due to the amplification of the
32 vertical component at frequencies higher than the fundamental one. Such high-frequency
33 amplification effects on the GIT Z component could also result if significant direct P-wave
34 energy is included in the chosen S-wave windows. This situation could occur if, by
35 selecting a time windows starting 1 sec before the S-wave onset, some late compressional
36 phases with significant amplitudes compared to the high-frequency S-wave part, or in the
37 worst case at stations close to the considered source, the entire P-wave arrival were
38 included the S-wave signal window. This effect is however not expected to be significant in
39 our case, since the hypocentral distances are always larger than 5 km (which roughly
40
41
42
43
44
45
46
47
48
49
50
51
52
53
54
55
56
57
58
59
60
61
62
63
64
65

1
2
3 corresponds to a minimum S-P travel time difference of 1 sec for typical upper crustal P-
4
5 wave velocities), with most data points obtained at hypocentral distances of 10 km or
6
7 larger. Furthermore, in the framework of the GIT methodology, the separation of source
8
9 spectra and site response relies on a set of records sampling different distances for each
10
11 earthquake and station. Finally, for stations showing only little amplification of the Z
12
13 component (e.g. CLT3 or CSG3), the H/V ratio provides an acceptable first order
14
15 approximation to the GIT H site response.
16
17
18
19

20 21 **DISCUSSION AND CONCLUSIONS**

22
23 Using the non-parametric GIT approach, we have investigated attenuation
24
25 characteristics, source spectra, and site response functions for the ISNet seismic network,
26
27 proving a means to better understand the influence of these different effects on ground
28
29 motion amplitudes.
30
31

32
33 We have determined non-parametric attenuation functions for 40 discrete frequencies
34
35 between 1 and 30 Hz. These functions generally show a relatively simple shape, with a
36
37 slight change in the rate of amplitude decay between 20 and 50 km. The quality factor Q
38
39 based on the S-wave part of the recordings shows a pronounced frequency-dependence
40
41 (close to linear), given by $Q(f) = 28.3f^{0.87}$. This S-wave attenuation model differs from the
42
43 results of other authors reported for neighboring regions (Rovelli *et al.*, 1988; Malagnini *et*
44
45 *al.*, 2000; Bianco *et al.*, 2002), and in particular shows a less severe frequency-dependence
46
47 than the results derived by Castro *et al.* (2004b, 2008) for southern Italy. However, as stated
48
49 above, it is important to keep in mind that the comparison of different models is
50
51 complicated by the fact that the data used to estimate them sample different frequency
52
53 bands and different crustal volumes. Nevertheless, the differences in Q estimates over the
54
55 range of different studies and regions under investigation indicate that a significant lateral
56
57
58
59
60
61
62
63
64
65

1
2
3 variability in seismic attenuation characteristics exists in Italy. Indeed, Zolezzi et al. (2008),
4
5 performing an attenuation tomography study of the southern Apennines, showed for
6
7 instance that the attenuation structure clearly differs on the Tyrrhenian side with respect to
8
9 the Adriatic side of the southern Apennines chain.
10

11
12
13 The earthquake spectra corrected for attenuation were used to derive source
14
15 parameters following the ω^2 -model (Brune, 1970, 1971), since the inverted source spectra
16
17 can be well explained with the ω^2 spectral shape. The obtained corner frequencies and
18
19 seismic moments provide indications that at least in the narrow magnitude range under
20
21 investigation, self-similar scaling seems to hold almost perfectly. However, we
22
23 acknowledge that of course the magnitude range $M_L=1.5-3.1$ is by far too small to speculate
24
25 upon any general scaling characteristics of earthquakes in the region. The stress drops range
26
27 from 0.01 to about 2 MPa, which is close to the lower bounds typically observed for crustal
28
29 earthquakes (0.1-100 MPa, e.g. Kanamori, 1994). Thus, the earthquakes under investigation
30
31 in this study seem to show only rather weak high-frequency energy radiation. This
32
33 conclusion is also compatible with the observation that the local magnitude M_L seems to
34
35 systematically underestimate M_W by about 0.5 magnitude units.
36
37
38
39
40
41
42

43 Finally, the results of the spectral inversion and the H/V analysis point out that only
44
45 few stations of the ISNet network are not noticeably affected by site effects. Such stations
46
47 are, as expected, located on rock sites. In addition, some stations located on what appears to
48
49 be competent rock show amplification in the high frequency range. This could be explained
50
51 by taking into account the effect of a near-surface, low-velocity layer due to the presence of
52
53 weathered rock, but also topographic effects might play a role. However, the unfortunately
54
55 rather poor knowledge of the geologic units below the stations does not allow for any
56
57
58
59
60
61
62
63
64
65

1
2
3 definitive conclusion, and in order to better understand how the observed amplification
4
5 effects are caused in detail, geotechnical information of subsurface structure is required.
6
7

8
9 As we have shown, the maximum amplification is generally shifted to higher
10 frequencies in the Z component as compared with the H component, and in some cases,
11 significant amplification effects are visible on the Z component. In such cases, S-P
12 conversions at the bottom of the soft layer could explain the simultaneously observed
13 reduction of the H/V amplitude due to this amplification on the Z component at frequencies
14 higher than the fundamental one, causing an increased disagreement between the GIT H
15 site response and H/V ratio function. Summarizing our site response results, we can hence
16 state that our observations are in good agreement with previous studies, in particular also
17 with respect to the comparison of GIT and H/V site response estimates (e.g., Field and
18 Jacob, 1995; Bonilla et al., 1997; Parolai et al., 2004), which have shown that the H/V
19 method provides a good estimate of the fundamental frequency of resonance of S-waves,
20 but often underestimates the level of amplification with respect to the GIT approach.
21
22
23
24
25
26
27
28
29
30
31
32
33
34
35
36
37

38 On the basis of our findings, we finally conclude that the results presented in this
39 study allow for an improved characterization of the seismic recordings obtained by the
40 ISNet network. This characterization is of particular importance since the data streams
41 recorded by the ISNet network are intended for usage in real-time seismic information
42 systems (i.e., early warning and near real-time shake map estimation, Iannaccone et al.,
43 2010), and our results provide a means to incorporate knowledge of the attenuation
44 structure, site effects modifying ground motions at the ISNet stations as well as potential
45 correction factors in magnitude estimation into these systems.
46
47
48
49
50
51
52
53
54
55
56
57

58 **ACKNOWLEDGMENTS**

59
60
61
62
63
64
65

1
2
3 The data used in this study were recorded by ISNet (Irpinia Seismic Network) managed by
4
5 Amra Scarl (Analisi e Monitoraggio del Rischio Ambientale) and are available online
6
7 through <http://isnet.na.infn.it/>. Data availability is subject to registration. Some of the
8
9 figures were drawn with the software Generic Mapping Tools (www.soest.hawaii.edu/gmt).
10
11 This work was performed during a three months visit of L. Cantore at the GFZ German
12
13 Research Centre for Geosciences in Potsdam, Germany, in the framework of a DAAD
14
15 (Deutscher Akademischer Austausch Dienst) grant. We would like to thank Marco
16
17 Mucciarelli and an anonymous reviewer for constructive comments that helped to improve
18
19 the manuscript.
20
21
22
23

24 REFERENCES

- 27 Anderson, J. and S. Hough (1984). A model for the shape of the Fourier amplitude
28
29 spectrum of acceleration at high frequencies. *Bull Seism. Soc. Am.* 74, 1969-1993.
30
31
32
33 Andrews, D. J. (1986). Objective determination of source parameters and similarity of
34
35 earthquakes of different size. *Geophysical Monographs* 37, 6, 259-267.
36
37
38 Archuleta, R. J., and J. H. Steidl (1998). ESG studies in the United States: results from
39
40 borehole arrays in *The Effects of Surface Geology on Seismic Motion*, K. Irikura, K.
41
42 Kudo, H. Okada, and T. Sasatani (editors) Vol. 1, Balkema, Rotterdam, 3-14.
43
44
45
46 Beresnev, I. A. (2001). What we can and cannot learn about earthquake sources from the
47
48 spectra of seismic waves. *Bull. Seismol. Soc. Am.* 91, 397-400.
49
50
51
52 Beresnev, I. A. (2002). Source parameters observable from the corner frequency of
53
54 earthquake spectra. *Bull. Seismol. Soc. Am.* 92, 2047-2048.
55
56
57 Bianco, F., E. Del Pezzo, M. Castellano, J. Ibanez, and F. Di Luccio (2002). Separation of
58
59 intrinsic and scattering seismic attenuation in the Southern Apennine zone, Italy.
60
61 *Geophys. J. Int.* 150 10-22.
62
63
64
65

- 1
2
3 Bernard, P., and A. Zollo (1989). The Irpinia (Italy) 1980 earthquake: Detailed analysis of a
4
5 complex normal faulting, *J. Geophys. Res.* B94, 1631–1647.
6
7
8 Bonilla, L. F., J. H. Steidl, G. T. Lindley, A. G. Tumarkin, and R. J. Archuleta (1997). Site
9
10 amplification in the San Fernando Valley, California: variability of site-effect
11
12 estimation using the S-wave, coda and H/V methods. *Bull. Seismol. Soc. Am.* 87,
13
14 710–730.
15
16
17
18 Brune, J. N. (1970). Tectonic stress and the spectra of seismic shear waves from
19
20 earthquakes. *J. Geophys. Res.* 75, 4997-5009.
21
22
23
24 Brune, J.N. (1971). Correction. *J. Geophys. Res.* 76, 5002.
25
26
27 Castro, R. R., J. G. Anderson, and S. K. Singh (1990). Site response, attenuation and source
28
29 spectra of S waves along the Guerrero, Mexico, subduction zone. *Bull. Seismol. Soc.*
30
31 *Am.* 80, 1481–1503.
32
33
34
35 Castro, R. R., F. Pacor, D. Bindi, G. Franceschina and L. Luzi (2004a): Site response of
36
37 strong motion stations in the Umbria, Central Italy, Region. *Bull. Seismol. Soc. Am.*
38
39 **94** (2), 576-590.
40
41
42
43 Castro, R. R., M.R. Gallipoli and M. Mucciarelli (2004b): An attenuation study in
44
45 Southern Italy using local and regional earthquakes recorded by seismic network of
46
47 Basilicata. *Annals of Geophys.* **47**(5), 1597-1608.
48
49
50
51 Castro, R.R., M.R. Gallipoli, and M. Mucciarelli (2008). Crustal Q in Southern Italy
52
53 determined from regional earthquakes. *Tectonophysics* 457, 96-101.
54
55
56 Cinti, F. R., L. Faenza, W. Marzocchi, and P. Montone (2004). Probability map of the next
57
58 $M \geq 5.5$ earthquakes in Italy. *Geochemistry, Geophysics, Geosystem*, 5, Q 11003, doi:
59
60 10.1029/2004GC000724.
61
62
63
64
65

- 1
2
3 Convertito, V., R. De Matteis, L. Cantore, A. Zollo and G. Iannaccone (2009). Rapid
4
5 estimation of ground-shaking maps for seismic emergency management in the
6
7 Campania region of Southern Italy. *Natural Hazards*, doi: 10.1007/s11069-009-9359-
8
9 2.
- 10
11
12 Efron, B., and R. J. Tibshirani (1994). *An Introduction to the Bootstrap*. Chapman and Hall,
13
14 London.
- 15
16
17 Emolo, A., G. Iannaccone, A. Zollo, and A. Gorini (2004). Inferences on the source
18
19 mechanisms of the 1930 Irpinia (southern Italy) earthquake from simulations of the
20
21 kinematic rupture process. *Ann. Geophys.* 47, 1743–1754.
- 22
23
24
25
26 Field, E. H., and K. H. Jacob (1995). A comparison and test of various site-response
27
28 estimation techniques, including three that are not reference-site dependent. *Bull.*
29
30 *Seism. Soc. Am.* 4, 1127-1143.
- 31
32
33
34 Hanks, T. C., and H. Kanamori (1979). A moment magnitude scale, *J. Geophys. Res.* 84,
35
36 2348–2350.
- 37
38
39 Hanks, T.C., and Thatcher, W. (1972). A graphical representation of seismic source
40
41 parameters. *J. Geophys. Res.*, 77(23), 4393-4405.
- 42
43
44 Iannaccone, G., Zollo, A., Elia, L., Convertito, V., Satriano, C., Martino, C., Festa, G.,
45
46 Lancieri, M., Bobbio, A., Stabile, T., Vassallo, M., and Emolo, A. (2010). A
47
48 prototype system for earthquake early-warning and alert management in southern
49
50 Italy. *Bull. Earthq. Eng.* 8, 1105-1129, doi:10.1007/s10518-009-9131-8.
- 51
52
53
54
55 Kanamori, H. (1994). Mechanics of earthquakes, *Ann. Rev. Earth Planet. Sci.* 22, 207–237.
- 56
57
58
59 Konno, K., and T. Ohmachi (1998). Ground-motion characteristics estimated from spectral
60
61 ratio between horizontal and vertical components of microtremor. *Bull. Seismol. Soc.*

- 1
2
3 Am. 88, 228–241.
4
5
6 Langston, C. A. (1979). Structure under Mount Rainier, Washington, inferred from
7
8 teleseismic body waves. *J. Geophys. Res.* 84, 4749-4762.
9
10
11 Lermo, J., and F. J. Chavez-Garcia (1993). Site effect evaluation using spectral ratios with
12
13 only one station. *Bull. Seism. Soc. Am.* 83, 1574-1594.
14
15
16 Malagnini, L., R. B. Herrmann and M. Di Bona (2000). Ground-motion scaling in the
17
18 Apennines (Italy). *Bull. Seismol. Soc. Am.*, **90** (4), 1062-1081.
19
20
21
22 Menke, W. (1989). *Geophysical Data Analysis: Discrete Inverse Theory*, International
23
24 Geophysics Series, Academic Press, New York.
25
26
27 Montone, P., M. T. Mariucci, S. Pondrelli, and A. Amato, (2004). An improved stress map
28
29 for Italy surrounding regions (central Mediterranean). *J. Geophys. Res.* 109, B10410,
30
31 doi: 10.1029/2003JB002703.
32
33
34
35 Nakamura, Y. (1989). A method for dynamic characteristics estimations of subsurface using
36
37 microtremors on the ground surface. *Q. Rep. Railway Tech. Res. Inst. Japan*, 30, 25-
38
39 33.
40
41
42
43 Oth, A., D. Bindi, S. Parolai, and F. Wenzel (2008). S-wave attenuation characteristics
44
45 beneath the Vrancea region in Romania: new insights from the inversion of ground-
46
47 motion spectra. *Bull. Seismol. Soc. Am.* 98, no. 5, 2482–2497, doi:
48
49 10.1785/0120080106.
50
51
52
53 Oth, A., Parolai, S., Bindi, D., and Wenzel, F. (2009). Source spectra and site response from
54
55 S waves of intermediate-depth Vrancea, Romania, earthquakes. *Bull. Seismol. Soc.*
56
57 *Am.* 99, 235-254, doi: 10.1785/0120080059.
58
59
60
61
62
63
64
65

- 1
2
3 Pantosti, D., and G. Valensise (1990). Faulting mechanism and complexity of the 23
4
5 November 1980, Campania-Lucania earthquake, inferred from surface observations.
6
7 J. Geophys. Res. 95, 15319–15341.
8
9
- 10 Parolai, S., D. Bindi, and P. Augliera (2000). Application of the generalized inversion
11
12 technique (GIT) to a microzonation study: numerical simulations and comparison
13
14 with different site-estimation techniques. Bull. Seismol. Soc. Am. 90, 286–297.
15
16
17
- 18 Parolai, S., and S. M. Richwalski (2004). The importance of converted waves in comparing
19
20 H/V and RSM site response estimates. Bull. Seismol. Soc. Am. 94, 304–313.
21
22
23
- 24 Parolai, S., D. Bindi, M. Baumbach, H. Grosser, C. Milkereit, S. Karakisa, and S. Zünbül
25
26 (2004). Comparison of different site response estimation techniques using aftershocks
27
28 of the 1999 Izmit earthquake. Bull. Seismol. Soc. Am. 94, 1096–1108.
29
30
31
- 32 Rovelli, A., O. Bonamassa, M. Cocco, M. Di Bona and S. Mazza (1988). Scaling laws and
33
34 spectral parameters of the ground motion in active extensional areas in Italy. Bull.
35
36 Seismol. Soc. Am., 78 (2), 530-560.
37
38
- 39 Steidl, J., A. G. Tumarkin, and R. J. Archuleta (1996). What is a reference site? Bull. Seism.
40
41 Soc. Am. 86, 1733-1748.
42
43
44
- 45 Theodulidis, N. and Bard, P.-Y. (1995). Horizontal to vertical spectral ratio and geological
46
47 conditions: an analysis of strong motion data from Greece and Taiwan. Soil. Dyn.
48
49 Earthquake Eng., 14,177–197.
50
51
52
- 53 Weber, E., V. Convertito, G. Iannaccone, A. Zollo, A. Bobbio, L. Cantore, M. Corciulo, M.
54
55 Di Crosta, L. Elia, C. Martino, A. Romeo, and C. Satriano (2007). An advanced
56
57 seismic network in the southern Apennines (Italy) for seismicity investigations and
58
59 experimentation with earthquake early warning. Seism. Res. Lett. 78, 622–534.
60
61
62

1
2
3
4
5
6
7
8
9
10
11
12
13
14
15
16
17
18
19
20
21
22
23
24
25
26
27
28
29
30
31
32
33
34
35
36
37
38
39
40
41
42
43
44
45
46
47
48
49
50
51
52
53
54
55
56
57
58
59
60
61
62
63
64
65

Westaway, R. (1987). The Campania, southern Italy, earthquakes of 1962 August 21.
Geophys. J. R. Astr. Soc. 8, 1–24.

Westaway, R., and J. Jackson (1987). The earthquake of 1980 November 23 in Campania-
Basilicata (southern Italy). Geophys. J. R. Astr. Soc. 90, 375–443.

Zolezzi, F., P. Morasca, K. Mayeda, W. S. Phillips, and C. Eva (2008). Attenuation
tomography of the Southern Apennines (Italy). J. Seismol. 12, 355–365.

TABLES

Table 1: S-wave attenuation models reported for Italy

Region	Frequency range (Hz)	Q-model	Geometrical spreading	Reference
Central and Central-southern Apennines	$0.1 \leq f \leq 20$	$Q(f) = 100 f$	$1/r$	Rovelli et al. (1988)
Entire Apennines	$0.24 \leq f \leq 5.0$	$Q(f) = 130 f^{0.1}$	$r^{-0.9}$, $r \leq 30$ km r^0 , $30 \leq r \leq 80$ km $r^{-0.5}$, $r \geq 80$ km	Malagnini et al. (2000)
Umbria-Marche	$0.3 \leq f \leq 9.5$	$Q(f) = 31.2 f^{1.2}$	$1/r$	Castro et al. (2004a)
Southern Italy	$1.6 \leq f \leq 10$	$Q(f) = 32.1 f^{1.7}$	$10/r^b$ $b=1.0 \pm 0.2$	Castro et al. (2004b)
Irpinia-Basilicata (southern Italy)	$1 \leq f \leq 30$	$Q(f) = 27.1 f^{0.95}$	$5/r$ (reference distance 5 km)	This study

Table 2: List of stations with the respective geological underground classification

CGG3	stiff soil
LIO3	stiff soil
CMP3	stiff soil
TEO3	stiff soil
CLT3	soft soil
RDM3	stiff soil
COL3	stiff soil
SCL3	stiff soil
CSG3	rock
PST3	stiff soil
SNR3	rock
AND3	rock
VDP3	stiff soil
STN3	rock
NSC3	rock
PGN3	stiff soil
SRN3	soft soil
VDS3	rock
BEL3	soft soil
RSF3	stiff soil
AVG3	rock
MNT3	stiff soil

FIGURE CAPTIONS

Figure 1. Stations of the ISNet seismic network used in this work. Grey circles indicate rock, black triangles stiff soil and open squares soft soil sites (see also Table 2). The solid black lines represent the surface projection of the three fault segments that ruptured during the 23 November 1980 earthquake (M 6.9).

Figure 2. Station locations (triangles), traces of fault segments (solid black lines), and source-station paths (grey lines) of the considered dataset. Two cross-sections through the epicentral area (one with latitude, one with longitude) are depicted as well.

Figure 3. a) Local magnitude M_L versus hypocentral distance R distribution for the dataset used in the inversion. b) Number of events with given M_L for the dataset used in the inversion.

Figure 4. Average H/V ratio calculated at station AND3. The grey-shaded area indicates the standard deviation. Note the approximately flat shape, with a slight rise above a value of 2 only at low frequencies.

Figure 5. a) Non-parametric attenuation functions (distance range 5-83 km) at 40 frequencies (1-30 Hz) obtained in the first step of the inversion scheme. The functions are color-coded with respect to the corresponding frequency (see legend). b) Two of the attenuation functions depicted in a) with their respective standard deviation from bootstrap analysis indicated as grey-shaded areas.

Figure 6. $Q(f)$ model derived from the analysis of the non-parametric attenuation functions shown in Figure 5 (solid black line). Dots and error bars indicate the individual Q -values obtained at each considered frequency, and the solid black line represents the fit to these data points of the form $Q(f)=Q_0f^N$. Other models from the literature are indicated in their

1
2
3 frequency range of validity (overlapping with our frequency range) for comparison (see
4
5 text).

6
7
8 **Figure 7.** Source results obtained from the spectral inversion. a) All source spectra (in
9 acceleration) as derived from the GIT inversion at a reference distance of $R_0=5$ km, color-
10 coded with respect to their M_L values. Green dashed lines indicate ω^2 model fits. b) Corner
11 frequency versus seismic moment plot. The grey line indicates a log-linear fit, with a slope
12 close to the expected theoretical value of $-1/3$ in the case of self-similar scaling. c) Stress
13 drop values computed as given in equation (6). d) Local magnitude M_L versus moment
14 magnitude M_W as estimated from the spectral fits shown in a). Note that M_L systematically
15 underestimates M_W by about 0.5 magnitude units.
16
17
18
19
20
21
22
23
24
25
26
27

28 **Figure 8.** Calculated GIT site response functions for six stations. The solid line indicates
29 the mean with the grey-shaded area depicting the standard deviation of 200 bootstrap
30 samples. The top panels are examples for stations classified as rock sites (see Table 2),
31 while the middle and bottom panels relate to stations classified as stiff and soft soil,
32 respectively.
33
34
35
36
37
38
39
40

41 **Figure 9.** Comparison of H/V ratios calculated directly from the ground motion spectra
42 (black lines with circles) and the GIT H/Z ratios (i.e. GIT site response on H component
43 divided by GIT site response on Z, black solid lines) for the same six stations as depicted in
44 Figure 8. The individual GIT site response functions for horizontal and vertical component
45 are indicated as well with grey lines with inverse triangles and squares, respectively.
46
47
48
49
50
51
52
53
54
55
56
57
58
59
60
61
62
63
64
65

Figure 1
[Click here to download high resolution image](#)

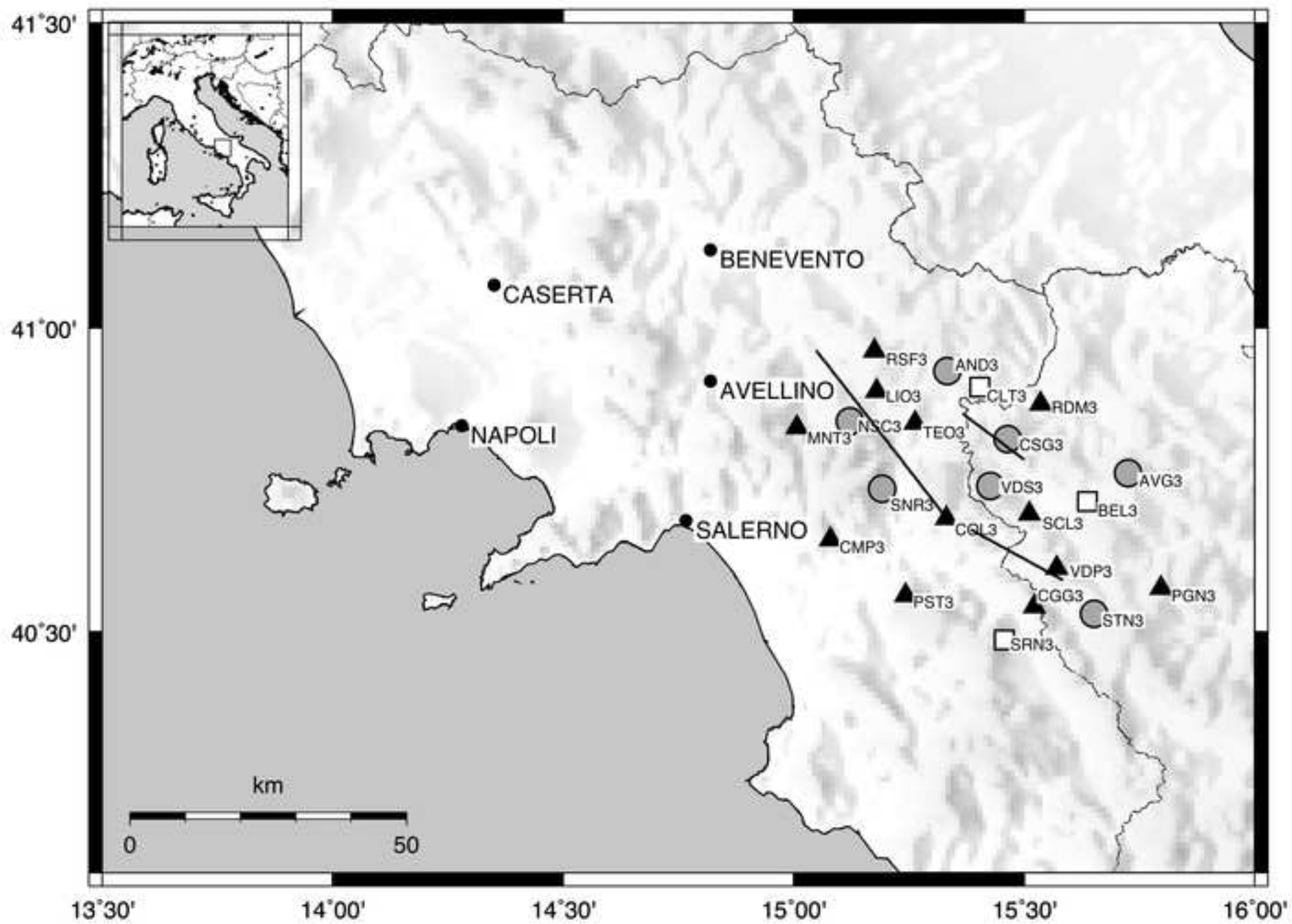


Figure 2

[Click here to download high resolution image](#)

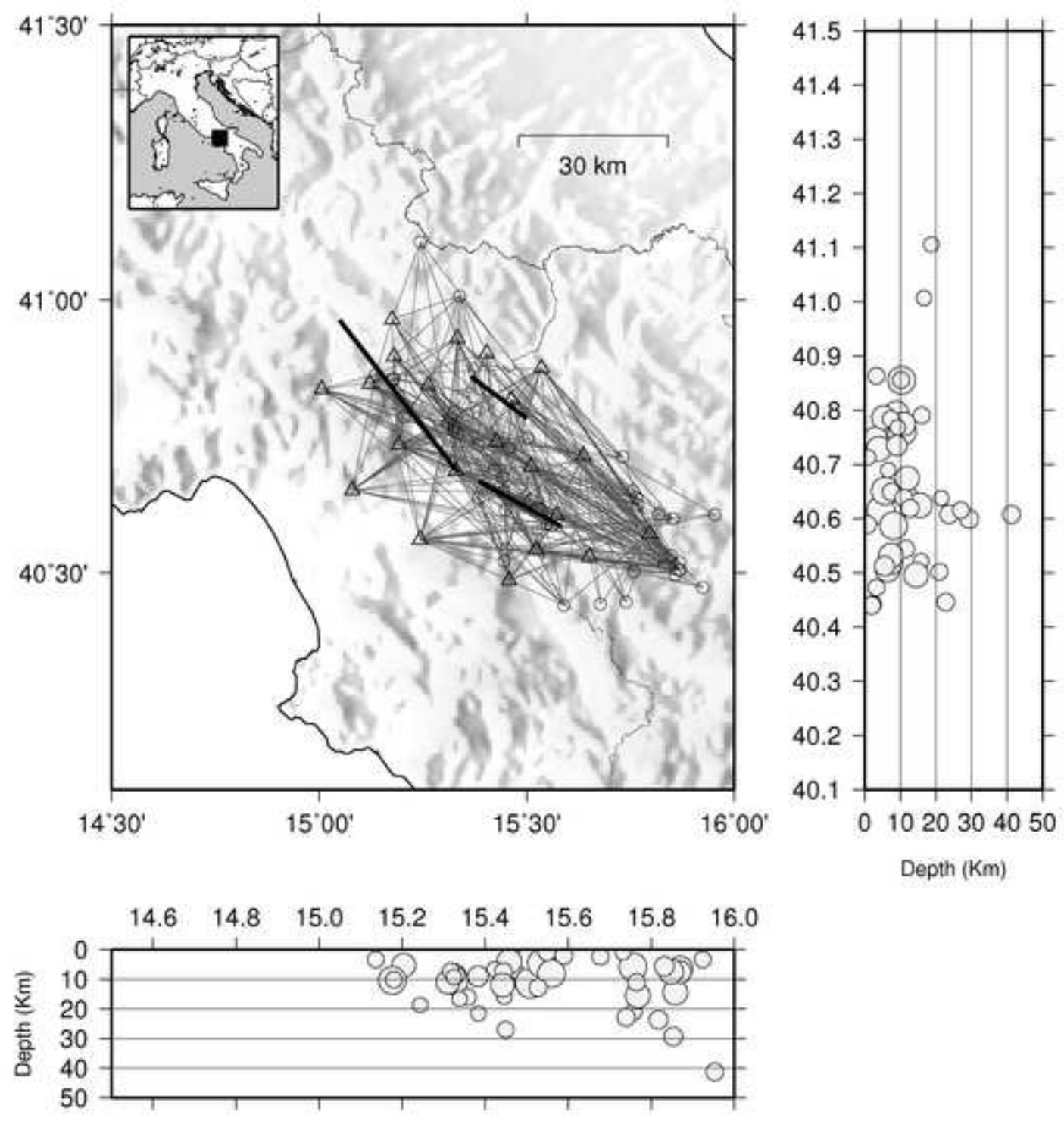


Figure 3
[Click here to download high resolution image](#)

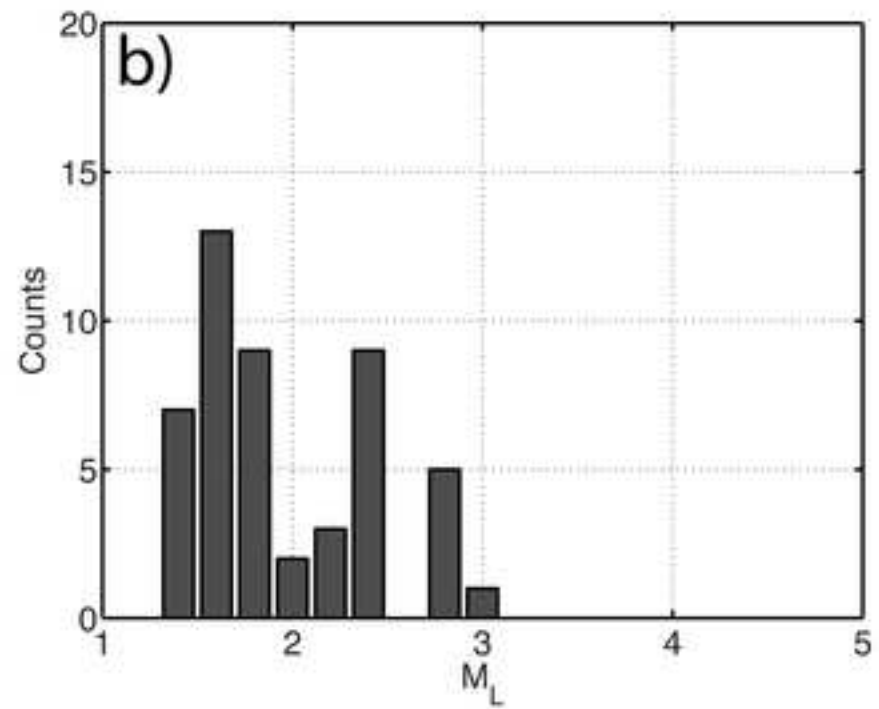
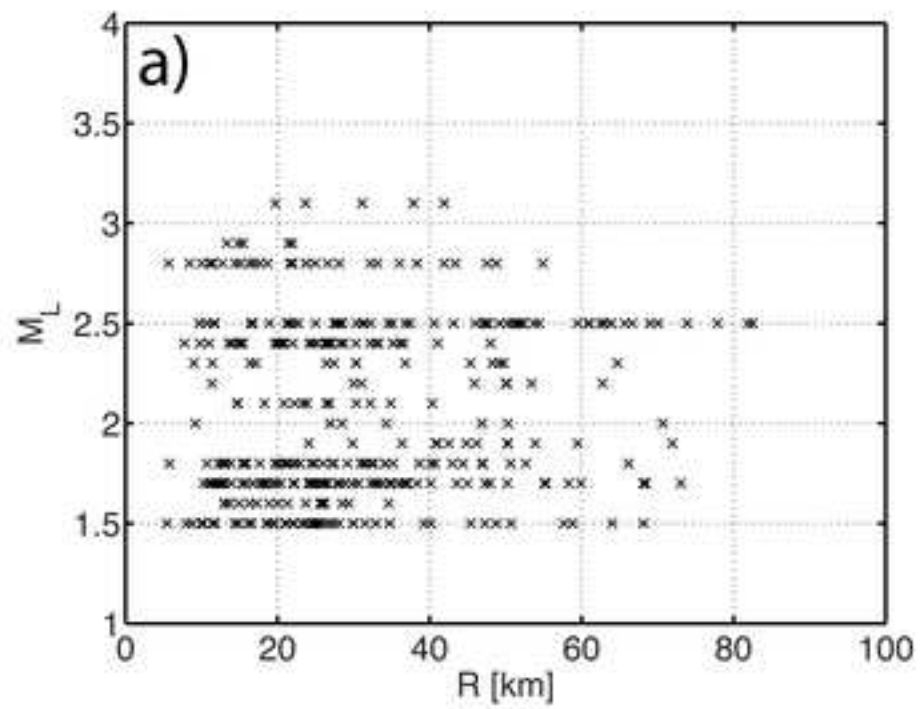


Figure 4
[Click here to download high resolution image](#)

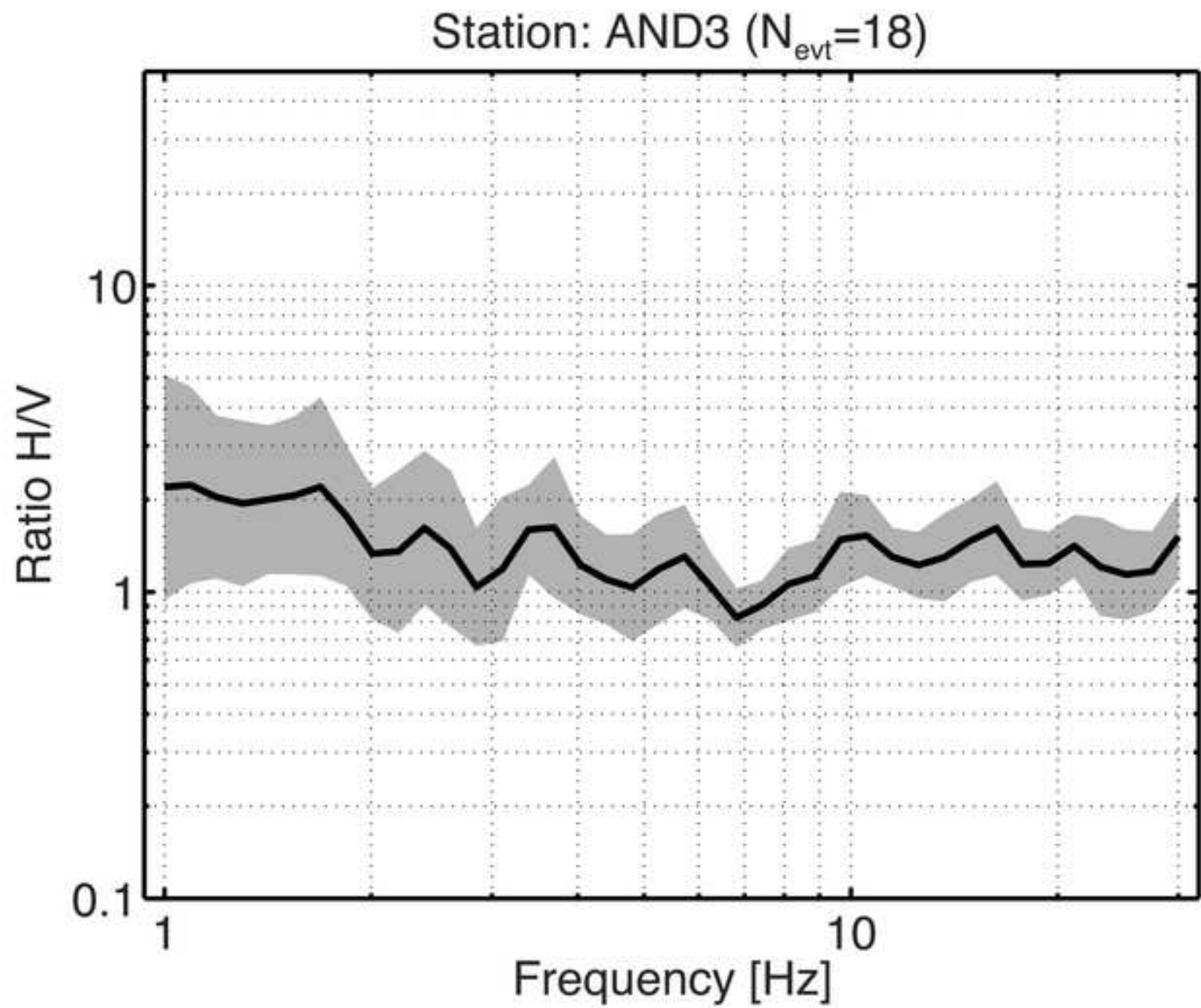


Figure 5
[Click here to download high resolution image](#)

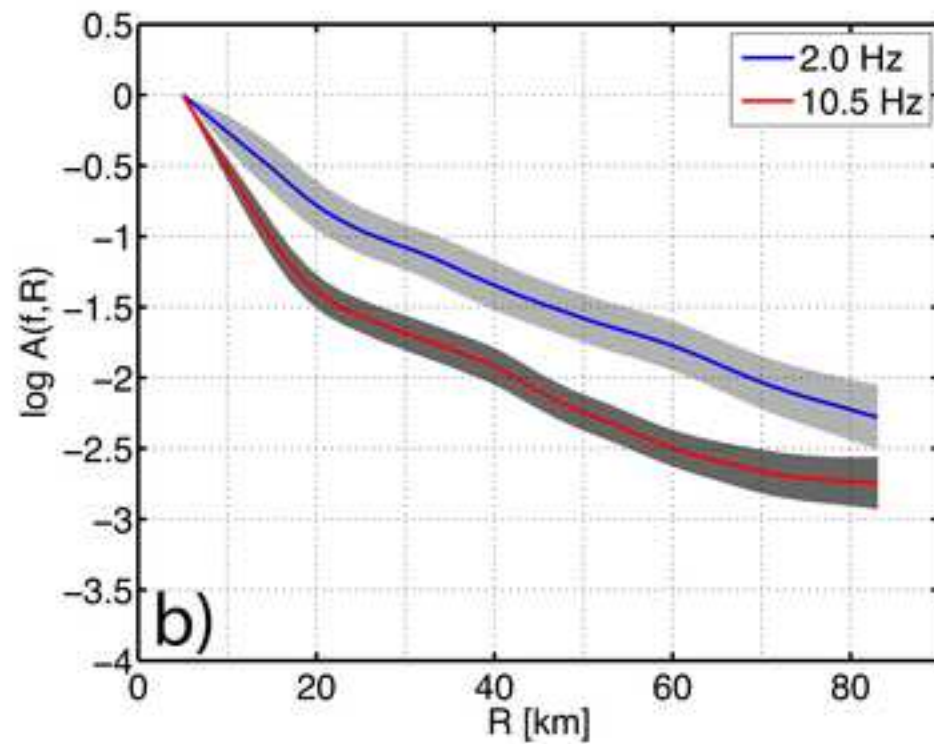
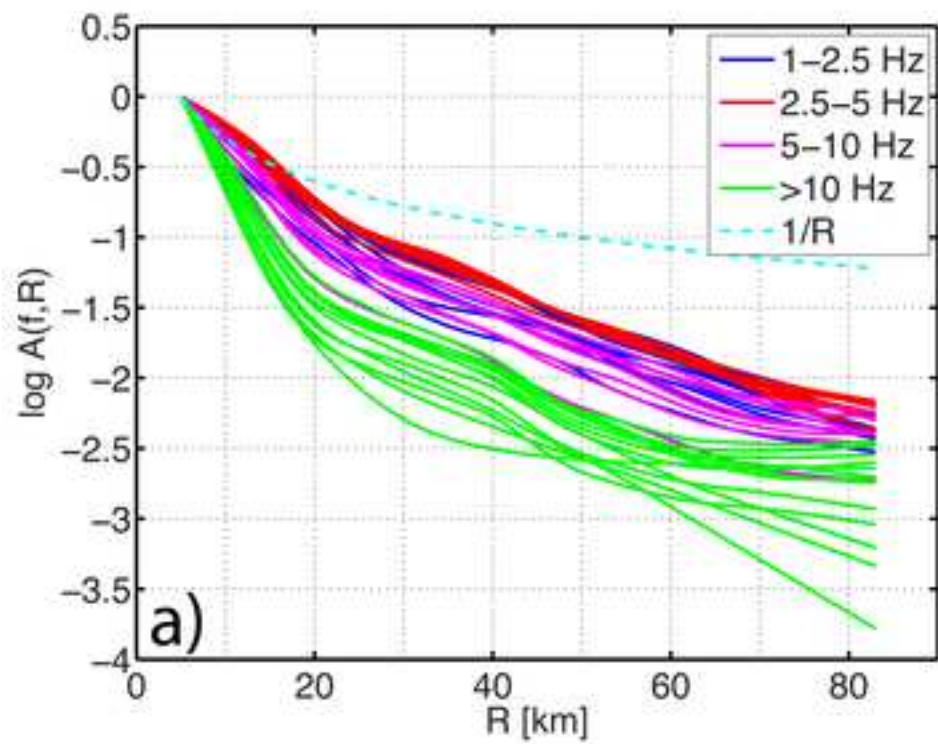


Figure 6
[Click here to download high resolution image](#)

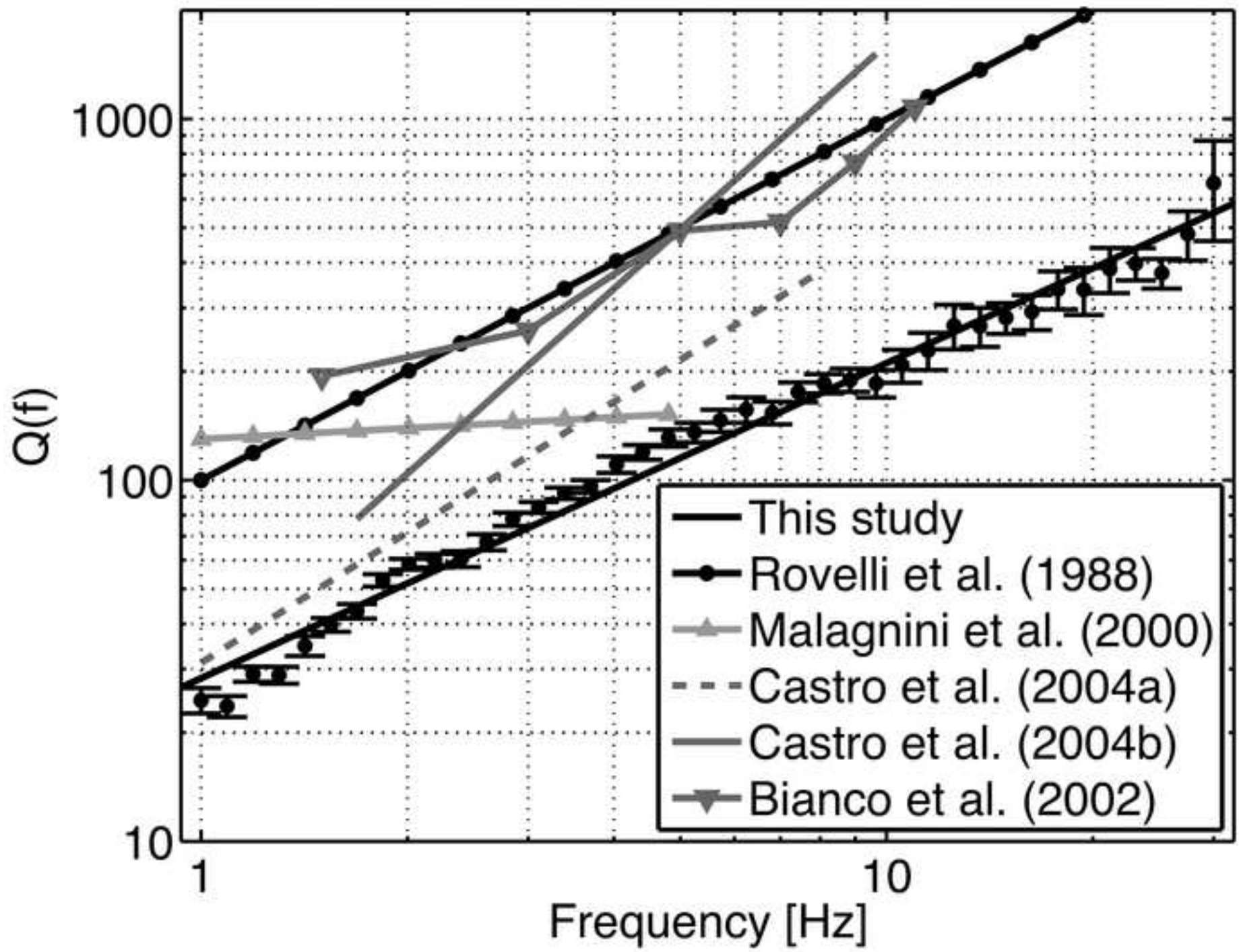


Figure 7
[Click here to download high resolution image](#)

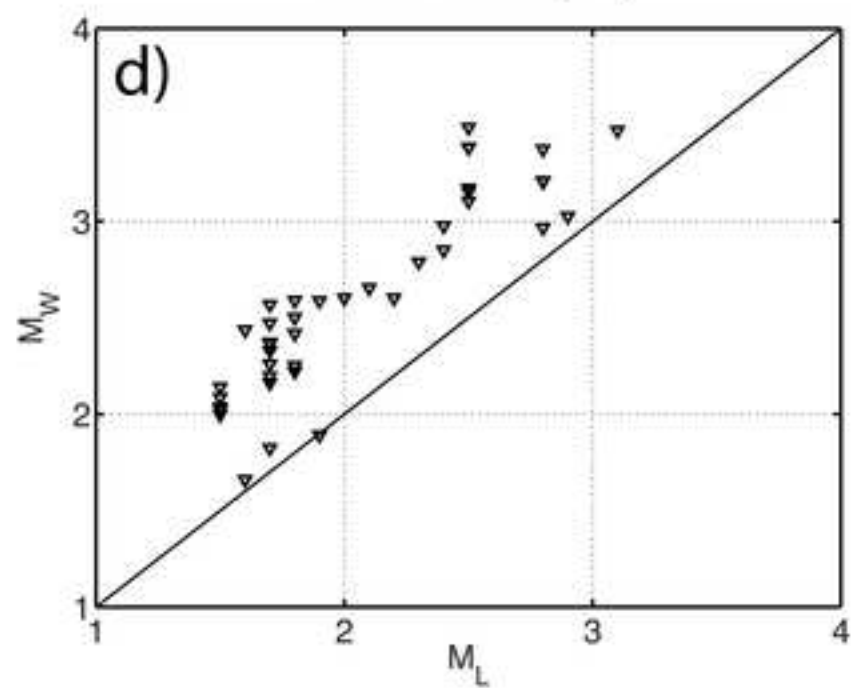
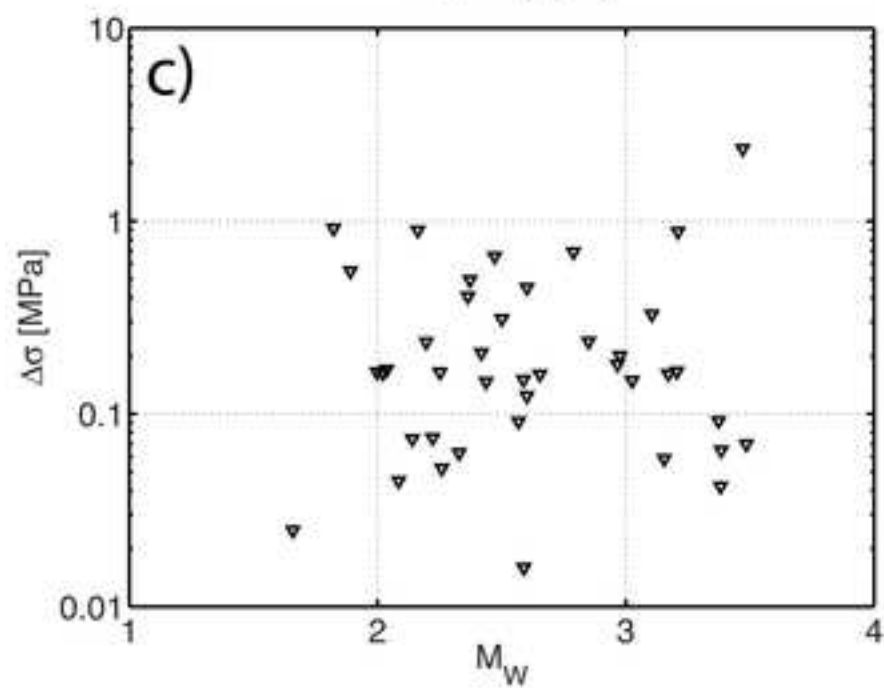
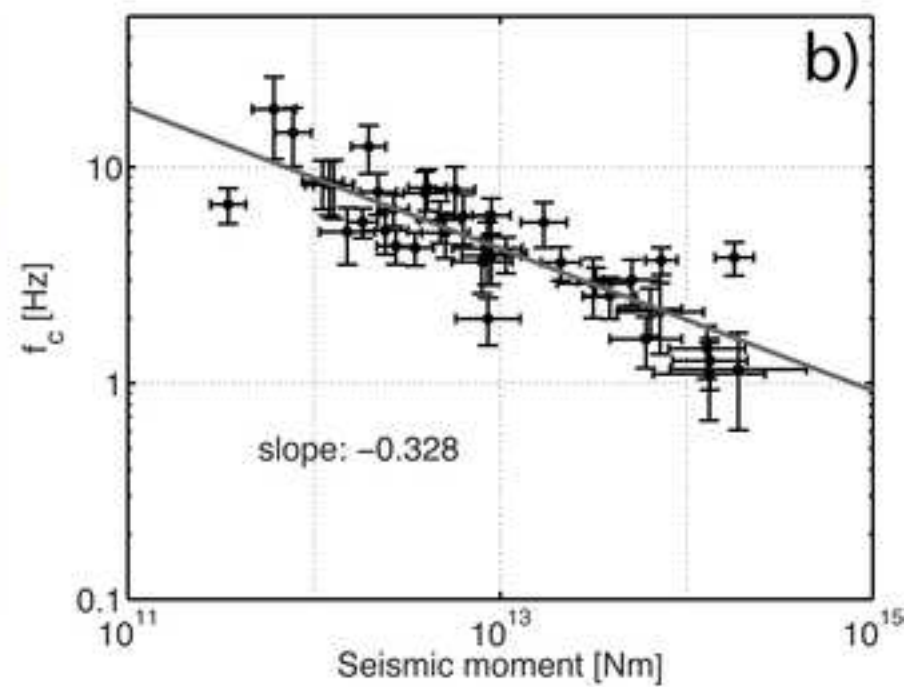
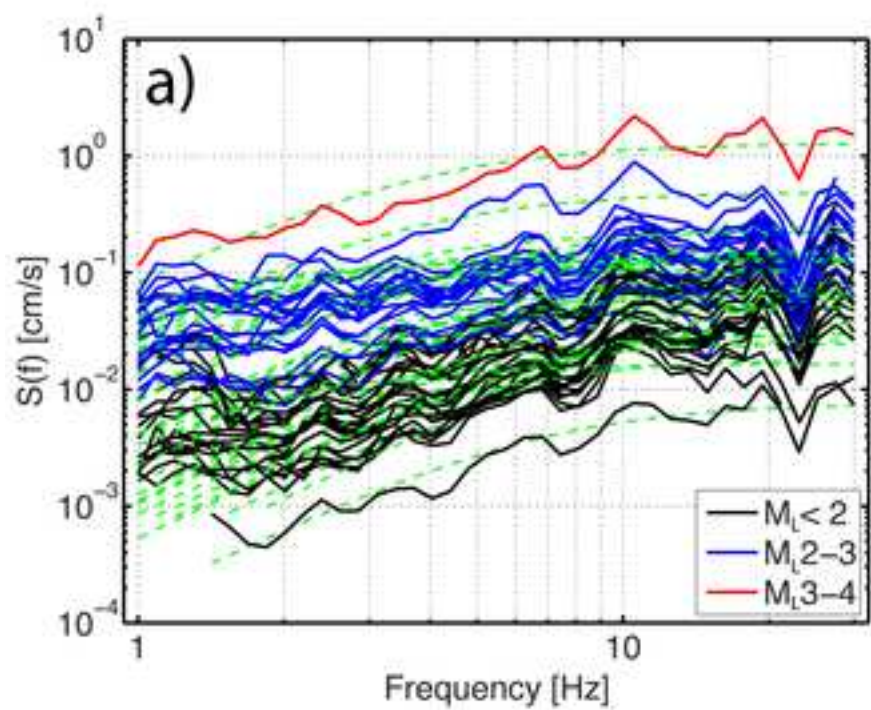


Figure 8
[Click here to download high resolution image](#)

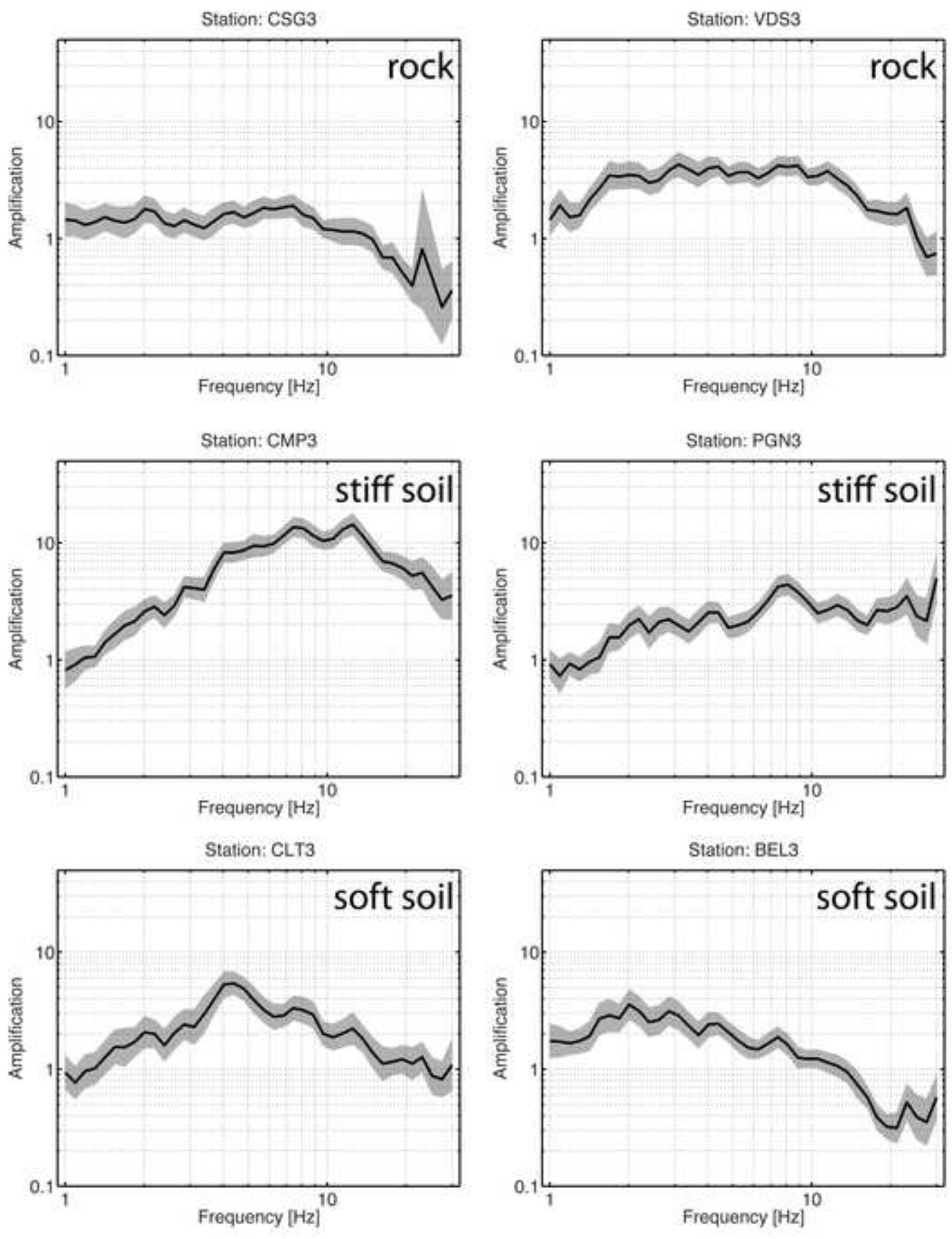
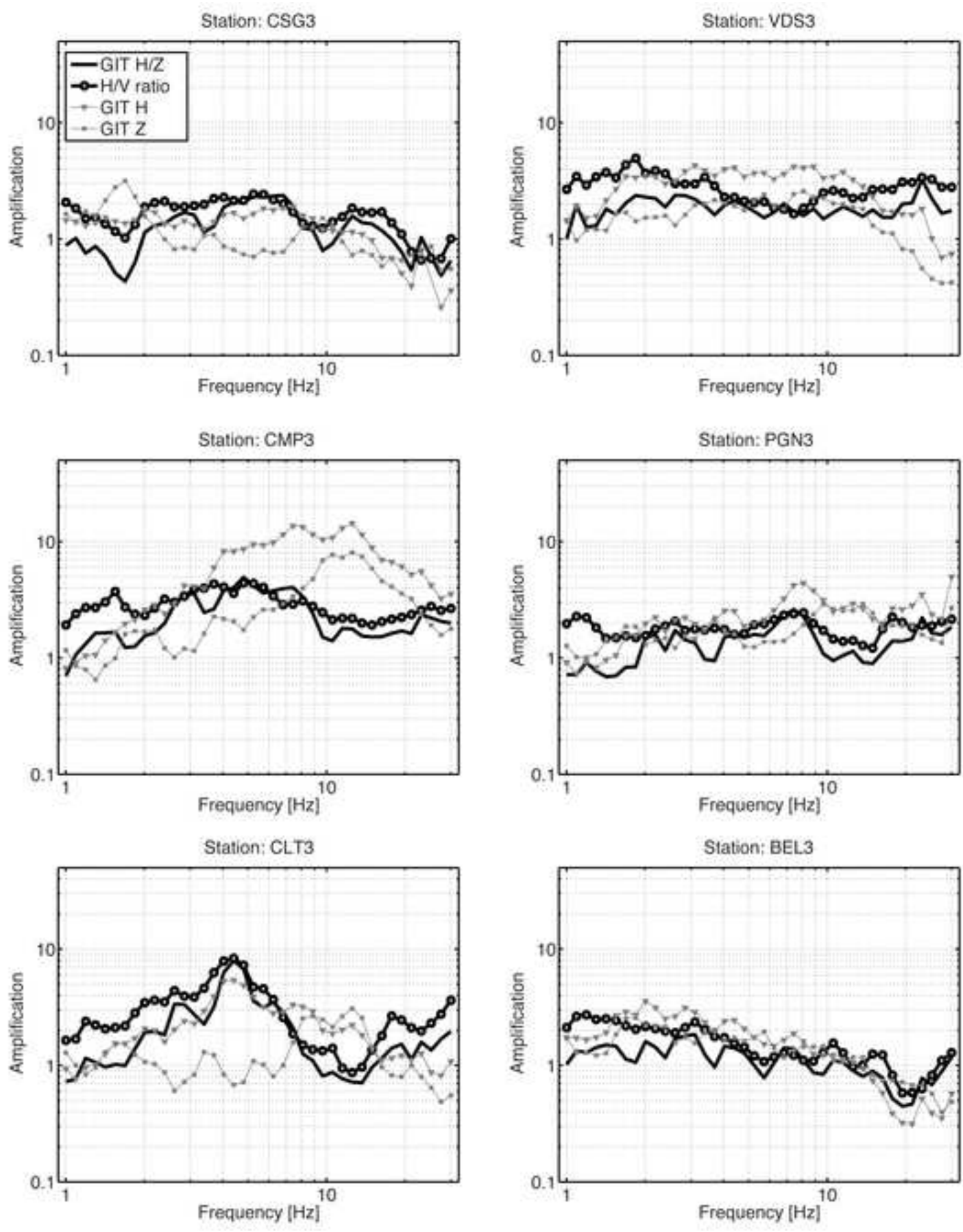


Figure 9
[Click here to download high resolution image](#)



Attenuation, source parameters and site effects in the Irpinia-Basilicata region (southern Apennines, Italy)

Luciana Cantore¹, Adrien Oth^{2,*}, Stefano Parolai³, Dino Bindi⁴

- 1) Dipartimento di Scienze Fisiche, Università degli Studi di Napoli Federico II, Naples I-80125, Italy.
- 2) European Center for Geodynamics and Seismology, rue Josy Welter 19, L-7256 Walferdange, Luxembourg
- 3) Helmholtz Centre Potsdam, GFZ German Research Centre for Geosciences, Earthquake Risk and Early Warning Section, Telegrafenberg, D-14473 Potsdam, Germany
- 4) Helmholtz Centre Potsdam, GFZ German Research Centre for Geosciences, Centre for Disaster Management and Risk Reduction Technology (CEDIM), Telegrafenberg, D-14473 Potsdam, Germany

*Corresponding author, adrien.oth@ecgs.lu

ABSTRACT

We derive S-wave attenuation characteristics, earthquake source parameters and site amplification functions at seismic stations used for earthquake early warning in the Irpinia-Basilicata region, using non-parametric spectral inversion of seismograms from 49 local events with $M_L=1.5-3.1$. We obtain relatively low Q -values ($Q_0=28$ at a frequency of 1 Hz) in conjunction with a strong frequency-dependence (close to linear). The source spectra can be satisfactorily modeled using the omega-square model, with stress drops ranging between 0.01-2 MPa, and in the narrow magnitude range available for analysis, the source spectra seem to scale self-similarly. The local magnitude M_L shows a linear correlation with moment magnitude M_W , however with a systematic underestimation by about 0.5 magnitude units. The results obtained in this work provide important insights into the ground motion characteristics that are required for appropriate seismic hazard assessment and are of practical relevance for a suite of applications, such as the calibration of ground-motion prediction equations or the correction for site amplification in earthquake early warning and rapid calculation of shake-maps for seismic emergency management.

Microsoft Office 1/16/11 9:43 PM

Deleted: through

Microsoft Office 1/16/11 9:44 PM

Deleted: a

INTRODUCTION

The southern Apennines represent an active tectonic region within Italy that accommodates differential motions between the Adria and Tyrrhenian microplates, responsible for almost all of the seismicity occurring in this region. Recent in situ stress data research (Montone et al., 2004) and seismological data analysis indicate that an extensional stress regime is prevalent in the southern Apennines, and that the seismic activity is confined to the narrow upper-crustal seismic zone. In particular, two main clusters of crustal earthquakes may be identified: the westernmost [cluster](#) with shallow earthquakes (depths < 20 km) along the axis chain (Irpinia area) and the easternmost [cluster](#) with deeper earthquakes (about 20-40 km) located on the outer margin of the chain (Potentino area) and the foredeep. The earthquakes in these two clusters show different focal mechanisms, indicating a pure extensional regime to the west (Irpinia) and a strike-slip regime to the east (Potentino).

During the last century, three large earthquakes with magnitudes [greater than 6](#) have occurred in [the](#) Irpinia-Basilicata region: the 1930 M 6.7 Irpinia earthquake (Emolo et al., 2004), the 1962 M 6.2 Irpinia earthquake (Westaway, 1987), and the 1980 M 6.9 Irpinia-Basilicata earthquake (Westaway and Jackson, 1987; Bernard and Zollo, 1989; Pantosti and Valensise, 1990). Particularly the 1980 Irpinia-Basilicata earthquake caused catastrophic damage [throughout the region](#), resulting in about 3,000 fatalities. Today, seismicity is mainly concentrated within or close to the fault system associated with the 1980 Irpinia-Basilicata earthquake, and several moderate-size events occurred in recent years, such as the 1990 and 1991 Potenza earthquakes (M 5.4 and 5.1, [within the deeper strike-slip zone](#)) and the 1996 event (M 4.9). This recent seismic activity provides clear indications that the Irpinia-Basilicata region still represents a region of high seismic risk, [now and in](#) the future

Microsoft Office 1/16/11 9:45 PM

Deleted: ,

Microsoft Office 1/16/11 9:45 PM

Deleted: above

Microsoft Office 1/15/11 6:06 PM

Deleted: to the city

Microsoft Office 1/16/11 9:46 PM

Deleted: ,

Microsoft Office 1/15/11 6:06 PM

Deleted:)

Microsoft Office 1/16/11 9:46 PM

Deleted: or

Microsoft Office 1/16/11 9:46 PM

Deleted: also

Microsoft Office 1/16/11 9:46 PM

Deleted: for

(Cinti et al., 2004).

In response to this threat, an earthquake early warning system prototype is in development in the Campania-Lucania region, the core of which is made up of the dense Irpinia Seismic Network (ISNet) recently installed along the southern Apennines chain (Figure 1). It is equipped with sensors that can provide high-quality recordings of both weak motions from small-magnitude events as well as strong ground shaking, thus enabling scientists to retrieve information about the rupture processes and to obtain insights into the scaling relationships between small and large events (Convertito et al., 2009). The network consists of 27 seismic instruments and covers an area of approximately 100x70 km² and has been especially designed to provide optimal coverage of the active fault system that generated the November 23 1980 Irpinia earthquake (Weber et al., 2007). Each station is equipped with a strong-motion accelerometer (Guralp CMG-5T) and a short period three-component seismometer (Geotech S13-J with natural period of 1 second), thus covering the entire necessitated dynamic recording range.

The ISNet seismic network was installed with the purpose of monitoring in real-time the potential source region of destructive earthquakes (i.e., the region around the source zone of the 1980 event) that, beyond the evident threat that these pose within the immediate source area, also represent a serious danger to the city of Naples and the densely populated coast. Thus, it is of utmost importance to provide the best possible characterization of the seismic recordings obtained at this local-scale network. One major aim of the work presented in this article is therefore to characterize the frequency-dependent site response for the ISNet stations by applying the generalized inversion technique (GIT) to the Fourier amplitude spectra (FAS) of ground motion. In addition to the information on site response, this technique provides us with insights into seismic attenuation characteristics within the

Microsoft Office 1/16/11 9:47 PM

Deleted: under

Microsoft Office 1/16/11 9:47 PM

Deleted: ,

Microsoft Office 1/16/11 9:47 PM

Deleted: particularly

Micro Soft 1/18/11 4:02 PM

Deleted: Since the intensity of shaking, and thus also the distribution of damage, is prone to be severely influenced by local site amplification effects, a thorough understanding and consideration of these is of particular importance for engineering and real-time seismological applications (i.e. early warning and rapid response).

Micro Soft 1/18/11 3:32 PM

Deleted: Therefore, o

Microsoft Office 1/16/11 9:48 PM

Deleted: Besides

Microsoft Office 1/16/11 9:48 PM

Deleted: , however

Microsoft Office 1/16/11 9:48 PM

Deleted: also

Micro Soft 1/18/11 3:35 PM

Deleted: of the area

1
2 area covered by the network, as well as source spectra of the utilized events, parameters that
3
4 are of considerable importance to better understand seismic ground motions in the area.

5
6 We first provide an overview of the dataset and the applied methodology, followed
7
8 by a discussion of seismic attenuation and, in particular, its frequency-dependence. From
9
10 the source spectra, we investigate the scaling characteristics in the available magnitude
11
12 range, derive the stress drops of the events and discuss the scaling relation between local
13
14 and moment magnitude. Finally, the site response functions for the ISNet stations are
15
16 discussed and compared to the H/V spectral ratios calculated directly from the ground
17
18 motion spectra.

20 DATASET

21
22 Seismograms from 49 local earthquakes that occurred between February 2006 and
23
24 November 2008 recorded by the short-period sensors of 22 ISNet stations constitute the
25
26 basis of our analysis. Data were recorded with a sampling rate of 125 samples per second,
27
28 and we only considered events and stations with at least 3 available recordings. For most
29
30 earthquakes and stations, however, more than 5 respectively 10 records could be used.

31
32 Figure 2 shows the station locations, the epicenters of the selected events, and the source-
33
34 station travel paths, which together show a satisfactory coverage of the area inside the
35
36 network. The hypocentral distances range from 5 to 83 km with best coverage between 10
37
38 to 65 km (Figure 3a), and the focal depths of the events are all shallower than 30 km. The
39
40 covered magnitude range is rather narrow ($1.5 < M_L < 3.1$) (Figure 3b), with the largest
41
42 number of events in the range $M_L = 1.5 - 2.5$.

43
44 The records were baseline corrected, the effect of instrumental response was removed
45
46 and the resulting seismograms were finally high-pass filtered applying a four-pole
47
48 Butterworth filter with corner frequency 0.2 Hz. For the purpose of our analysis, only the
49

Micro Soft 1/18/11 3:20 PM
Deleted:
Microsoft Office 1/16/11 9:48 PM
Deleted: with
Micro Soft 1/18/11 3:33 PM
Deleted: ,

Microsoft Office 1/16/11 9:49 PM
Deleted: and
Microsoft Office 1/16/11 9:48 PM
Deleted: ,
Microsoft Office 1/16/11 9:49 PM
Deleted: are indicated as well
Microsoft Office 1/16/11 9:50 PM
Deleted: ing
Microsoft Office 1/15/11 6:07 PM
Deleted: lower

1 S-wave portions of the records were used. Time windows starting 1 sec before the S-wave
2 onset (picked on the horizontal components) with a length of 5 sec were extracted. Before
3 calculation of the FAS, the beginning and end of each window were tapered with a 5%
4 cosine window, and the computed spectra were smoothed around 40 frequency points
5
6
7
8
9
10
11
12
13
14
15
16
17
18
19
20
21
22
23
24
25
26
27
28
29
30
31
32
33
34
35
36
37
38
39
40
41
42
43
44
45
46
47
48
49
50
51
52
53
54
55
56
57
58
59
60
61
62
63
64
65

Microsoft Office 1/16/11 9:50 PM
Deleted: ,

Microsoft Office 1/16/11 9:50 PM
Deleted: of equal

Microsoft Office 1/16/11 9:50 PM
Deleted: ,

METHODS

In order to separate source spectra, attenuation characteristics and site response functions from one another, we applied a two-step non-parametric spectral inversion scheme as originally proposed by Castro et al. (1990) (termed below as generalized inversion technique, GIT) to the velocity spectra of the ISNet S-wave records. We applied the GIT inversion both to horizontal and vertical components and compared the site response functions obtained by the GIT inversion with the H/V ratios calculated directly from the observed ground motion spectra at each station.

Generalized inversion technique (GIT)

Since the applied GIT approach is commonly used in the literature (e.g. Castro et al., 1990; Parolai et al., 2000, 2004; Oth et al., 2008, 2009), we limit our discussion on the methodology to the basic concept and refer the reader to the latter publications for the details. We followed the two-step procedure introduced by Castro et al. (1990): in the first

1
2 step, the dependence of the spectral amplitudes on distance for a given frequency f is given
3
4 by

$$5 \quad U_{ij}(f, r_{ij}) = A(f, r_{ij}) \cdot \hat{S}_j(f), \quad (1)$$

6
7
8
9 where $U_{ij}(f, r_{ij})$ represents the observed spectral amplitude at the i -th station resulting from
10 the j -th earthquake, r_{ij} is the source-site distance, $A(f, r_{ij})$ is the non-parametric attenuation
11 function, and $\hat{S}_j(f)$ is a scalar factor that depends on the size of the j -th source. In this
12 model, the functional form of $A(f, r_{ij})$ is not pre-defined and implicitly includes all effects
13 causing attenuation along the travel path (geometrical spreading, anelasticity, scattering,
14 etc.). Since the properties causing attenuation within the Earth's crust are thought to vary
15 slowly with distance, $A(f, r_{ij})$ is constrained to be a smooth decaying function with distance
16 r and to take the value $A(f, R_0) = 1$ at a specific reference distance R_0 (5 km in our case).
17 Site effects are not included in the formulation given by equation (1) and are supposed to be
18 primarily absorbed into the residuals of the observed ground motion spectra from this
19 parameterization.
20
21
22
23
24
25
26
27
28
29
30

31 For N spectral records, equation (1) represents a linear system of N equations, which
32 is formed for each frequency analyzed by taking the logarithm. The system of equations is
33 solved using singular value decomposition (Menke, 1989), providing us with discretized (in
34 bins of 2 km) attenuation functions $A(f, r_{ij})$ and the source scaling factors.
35
36
37
38
39

40 Estimates of the quality factor can be obtained through fitting a parametric model to
41 $A(f, r)$:
42
43

$$44 \quad A(f, r) = G(r) \exp\left(-\frac{\pi f r}{Q(f) v_s}\right). \quad (2)$$

1
2 Herein, $Q(f)$ is the S-wave quality factor, v_s the average shear wave velocity and $G(r)$
3
4 represents the geometrical spreading function. Since at distances larger than 70 km the
5
6 attenuation functions are only constrained by very few data points, we only used the
7
8 attenuation functions within distances lower than 70 km to derive $Q(f)$, setting the
9
10 geometrical spreading function to $G(r)=5/r$. From equation (2), $Q(f)$ can be evaluated from
11
12 the slope of a linear least-squares fit to $\log A(f,r)-\log G(r)$ versus distance. Finally, we
13
14 investigate the frequency dependence of Q assuming a model of the form $Q(f) = Q_0 f^N$.

15
16 After the attenuation functions $A(f, r_{ij})$ have been determined, the spectral amplitudes
17
18 at each frequency are corrected for the effect of seismic attenuation and in the second
19
20 inversion step, the corrected spectra are separated into source and site effects (Andrews,
21
22 1986):

$$23 \quad 24 \quad 25 \quad 26 \quad 27 \quad 28 \quad 29 \quad 30 \quad 31 \quad 32 \quad 33 \quad 34 \quad 35 \quad 36 \quad 37 \quad 38 \quad 39 \quad 40 \quad 41 \quad 42 \quad 43 \quad 44 \quad 45 \quad 46 \quad 47 \quad 48 \quad 49 \quad 50 \quad 51 \quad 52 \quad 53 \quad 54 \quad 55 \quad 56 \quad 57 \quad 58 \quad 59 \quad 60 \quad 61 \quad 62 \quad 63 \quad 64 \quad 65$$

$$R_{ij}(f) = S_j(f) \cdot Z_i(f). \quad (3)$$

Here, $R_{ij}(f) = U_{ij}(f, r_{ij}) / A(f, r_{ij})$ are the residual spectral amplitudes after correction
for path effects, $S_j(f)$ is the source spectrum of the j-th earthquake, and $Z_i(f)$ the site
amplification function at the i-th station. Equation (3) can be linearized as well by applying
the logarithm.

As noted by Andrews (1986), equation (3) still contains one undetermined degree of
freedom due to the linear dependence between site and source terms. This degree of
freedom must be fixed by setting a reference condition either for at least one source or one
site in the dataset. Usually, the site response of a rock site is fixed to one (respectively zero
in \log_{10}), irrespective of frequency, or the average site response at a set of competent sites is
set to unity.

We solved the second inversion by constraining the logarithm of the site

1
2 | amplification of a reference site to zero. We adopted station AND3 as [the](#) reference site
3
4 | because it is located on outcropping bedrock and the H/V ratio at this station is flat and
5
6 | almost equal to one over the entire analyzed frequency range (Figure 4), except at [the](#)
7
8 | lowest frequencies where there is a slight increase to a factor of about two. In order to
9
10 | evaluate the stability of the solution and estimate standard errors for the model parameters,
11
12 | we performed 200 bootstrap inversions (Efron and Tibshirani, 1994) for each of the 40
13
14 | frequency points following the same procedure as used by Parolai et al. (2000, 2004) and
15
16 | Oth et al. (2008, 2009). From the 200 bootstrap samples, the mean and standard error were
17
18 | calculated for each model parameter.

20 **H/V ratios of earthquake data**

21
22 | The GIT site responses have been compared with those calculated by horizontal-to-
23
24 | vertical (H/V) ratios derived from earthquake data. The H/V method, originally introduced
25
26 | by Nakamura (1989) to interpret microtremor recordings, has become a very popular tool in
27
28 | site response estimation in recent years. Lermo and Chavez-Garcia (1993) first applied this
29
30 | technique to the S-wave part of earthquake recordings as well. The H/V method, in analogy
31
32 | to the so-called receiver-function technique used to investigate the crustal and upper mantle
33
34 | structures from teleseismic records (Langston, 1979), assumes that the vertical component
35
36 | of ground motion is mainly controlled by source and attenuation effects and is not very
37
38 | sensitive to local site amplification. Thus, by deconvolving, or dividing in the frequency
39
40 | domain, the vertical component from the horizontal one, an estimate of the site response
41
42 | function can be obtained. Because the S-wave amplification at the surface depends on the
43
44 | angle of incidence (Lermo and Chavez-Garcia, 1993), it is necessary to average over a
45
46 | sufficient number of events distributed around the station of interest with good azimuthal
47
48 | and distance coverage in order to obtain stable estimates (Parolai et al., 2004).

1
2 Generally, comparisons of site response functions obtained with different techniques
3
4 (e.g., Field and Jacob, 1995; Bonilla et al., 1997; Parolai et al., 2004) have shown that the
5
6 H/V method provides a good estimate of the fundamental frequency of resonance, but
7
8 underestimates the level of amplification with respect to the GIT. Recently, Parolai and
9
10 Richwalski (2004) showed that the observed differences in the estimated amplifications
11
12 obtained applying different techniques could be linked to S-P conversions at the bottom of
13
14 the soft layer in the case of high impedance contrasts.

15 RESULTS

16 Attenuation characteristics

17
18 The obtained non-parametric attenuation functions at all 40 frequency points are
19
20 depicted in Figure 5a, color-coded with respect to their frequency, while in Figure 5b, two
21
22 of the attenuation curves are depicted together with their estimated standard deviation from
23
24 the bootstrap analysis. The latter plot shows that in general, the attenuation curves are well
25
26 constrained. The functions depict a relatively simple shape, being all monotonically
27
28 decaying with a change in the rate of amplitude decay for hypocentral distances between 20
29
30 and 50 km at higher frequencies. Below 20 km distance, the high frequencies show a
31
32 stronger decay with distance, while between 20 and 50 km, the slope of the attenuation
33
34 curves adjusts to be very similar for almost the entire frequency band.
35
36
37

38 Figure 6 shows the values of $Q(f)$ estimated for all frequencies using equation (2) (the
39
40 vertical error bars indicate the regression error of fit) and the least-squares fit of a relation
41
42 of the form $Q(f) = Q_0 f^N$ obtained with these values (solid black line). As can be seen from
43
44 Figure 6, the frequency-dependence of $Q(f)$ can be well approximated with a power-law
45
46 dependency given as:
47
48
49

$$Q(f) = 28.3f^{0.87}. \quad (4)$$

We thus find a rather strong frequency-dependence of the quality factor in the region. Other models derived for different regions in Italy, including southern Italy where the region under investigation by this study is located, are indicated in Figure 6 as well (within the overlap of the frequency range of their validity and the range 1-30 Hz of our study, see also Table 1). In particular, Castro et al. (2004b) derived the relationship $Q(f) = 32.1f^{1.7}$ from a dataset of 32 earthquakes recorded at 4 stations of the Basilicata seismic network. They obtained a much stronger frequency-dependence with $N > 1$, while in contrast the value of Q_0 is rather close to the one found here. [Castro et al. \(2008\) corroborated the results of Castro et al. \(2004b\), using a significantly extended dataset from the same seismic network. They furthermore used a more sophisticate analysis procedure on their non-parametric attenuation curves, providing separate estimations of upper und lower crustal attenuation characteristics in the frequency range 1-25 Hz. Assuming body-wave geometrical spreading \(\$\propto 1/r\$ \) over the first 50 km, they obtained the Q-model \$Q\(f\) = 18.8f^{1.7}\$ for the upper crust \(depth < 13 km\). While this frequency dependence is identical to one obtained by Castro et al. \(2004b\), attenuation is slightly larger at all frequencies due to the lower \$Q_0\$ value \(18.8 vs. 32.1\). Considering however the typical uncertainty ranges in determining such \$Q\(f\)\$ models, the results of both studies are highly consistent with one another, and we only list the result of Castro et al. \(2004b\) in Table 1 and Figure 6.](#) Another study covering the region of interest investigated coda- Q in the frequency range 1-12 Hz (Bianco et al., 2002) and the authors found from a multi lapse time window analysis that intrinsic Q seems to dominate with respect to scattering Q in the area. Other Q -models have been reported for different regions of Italy by Rovelli et al. (1988), Malagnini et al. (2000) and Castro et al. (2004a,b), and the one that matches our

Unknown
Field Code Changed

Microsoft Office 1/15/11 5:41 PM
Formatted: Subscript, Kern at 12 pt

Microsoft Office 1/16/11 9:58 PM
Deleted: ,

1
2 results most closely is the model for Umbria given by Castro et al. (2004a), with a
3
4 frequency-dependence $N=1.2$. It is important to point out that due to the trade-off between
5
6 Q and the geometrical spreading function, a reliable comparison between the different
7
8 models only makes sense if the estimates of Q are made using similar geometrical
9
10 spreading functions. Moreover, it should be noted that the data used to retrieve the
11
12 attenuation models listed in Table 1 sample different frequency bands and different crustal
13
14 volumes. The studies by Malagnini et al. (2000) and Rovelli et al. (1988) sample for
15
16 instance large regions such as the entire Apennines or the entirety of southern Italy. In
17
18 contrast, our results are related to a small area limited by the extent of [the ISNet network](#),
19
20 and also Bianco et al. (2002) analyzed data from a much larger area surrounding [the ISNet](#)
21
22 [network](#). This limitation of our study to the small region covered by [the ISNet network](#) can
23
24 however also be seen as an advantage in the sense that with the derived attenuation
25
26 functions, we provide a means for reliable and consistent attenuation correction for events
27
28 occurring in close proximity or within the network, avoiding a bias in source parameter or
29
30 site response estimation due to inappropriate attenuation correction.

31 **Source spectra**

32
33
34 In order to remove the undetermined degree of freedom when separating source
35
36 spectra and sites response from the attenuation-corrected spectral amplitudes as described
37
38 by equation (3), we fixed the site response at the reference station AND3 to unity,
39
40 irrespective of frequency. Since with the non-parametric attenuation functions discussed
41
42 above, we can only correct for attenuation up the reference distance of 5 km (i.e. the lowest
43
44 distance in our dataset), the obtained source spectra from the second inversion step are also
45
46 given at the reference distance of 5 km.

1
2 We did not include a term accounting for potential high-frequency decay due to the
3 exponential κ -operator (Anderson and Hough, 1984) in the reference condition, and it may
4 therefore be the case that some high-frequency decay due to near-surface high-frequency
5 diminution at the reference site is systematically shifted into the source spectra. In order to
6 investigate this issue, we plot the source spectra in acceleration (Figure 7a) and visually
7 checked the high-frequency part of the spectra. As can be seen from Figure 7a, the
8 acceleration source spectra generally show a clear plateau-like structure at highest
9 frequencies, as would be expected in the case the ω^2 -model (Brune, 1970, 1971) is valid.
10 Thus we cannot see any clear indication that a systematic high-frequency decay is moved
11 into the source contributions. There is one systematic through appearing in the source
12 spectra at a frequency of about 22-23 Hz, which may be due to an amplification effect at
13 the reference station not accounted for in the inversion constraint.

14
15 In order to derive the source parameters (i.e. seismic moments and corner
16 frequencies) of the 49 earthquakes in our dataset, we fitted the ω^2 -model to the inverted
17 source spectra (in acceleration, using the results from the horizontal component inversion)
18 using non-linear least squares:

$$S(f) = (2\pi f)^2 \cdot \frac{R^{\theta\phi}VF}{4\pi\rho v_s^3 R_0} \cdot M_0 \cdot \left[1 + \frac{f^2}{f_c^2} \right]^{-1}, \quad (5)$$

19 where $R^{\theta\phi}$ is the average radiation pattern set to 0.55, $V=1/\sqrt{2}$ accounts for the separation
20 of S-wave energy on two horizontal components, $F=2$ is the free surface amplification,
21 $\rho=2.8 \text{ g/cm}^3$ is the density, and $v_s = 3.3 \text{ km/sec}$ is the estimated average shear-wave
22 velocity in the source region. $R_0=5 \text{ km}$ represents the reference distance, M_0 denotes the
23 seismic moment, and f_c is the corner frequency. Finally, we compute stress drop estimates
24 from the moment and corner frequencies following Hanks and Thatcher (1972):

Microsoft Office 1/16/11 10:02 PM
Deleted: Since w

Microsoft Office 1/16/11 10:03 PM
Deleted: evaluate this effect

Microsoft Office 1/16/11 10:03 PM
Deleted:

Microsoft Office 1/16/11 10:03 PM
Deleted: -

Microsoft Office 1/16/11 10:05 PM
Deleted:

$$\Delta\sigma = 8.5 \cdot M_0 \cdot \left(\frac{f_c}{v_s} \right)^3. \quad (6)$$

The ω^2 fits to the inverted source spectra are indicated in Figure 7a as dashed green lines, showing that the source spectra can satisfactorily be explained using the ω^2 -model.

Figure 7b shows corner frequency plotted versus seismic moment (on a log-log scale), with the regressional errors of fit (obtained when fitting equation (5) to the source spectra)

indicated as horizontal respectively vertical error bars. In the case of self-similar scaling,

the relationship $M_0 \propto f_c^{-3}$ holds, and the slope of a fitted straight line in Figure 7b should

be close to -1/3. Indeed, we note that this is approximately the case, but at the same time, it

is clear that the magnitude range under investigation in this article is much too small to

draw any general conclusions on this issue. The stress drops derived using equation (6)

range between 0.01 and 2 MPa (Figure 7c). While this is still within the bounds generally

found for crustal earthquakes (~0.1-100 MPa, e.g. Kanamori, 1994), the values clearly

range at the bottom of this range, indicating comparatively low stress drops for the small

earthquakes in this area. Since earthquakes with low stress drops radiate only little high-

frequency energy as compared with high stress drop events, this observation can also

explain the fact that the local magnitude M_L generally underestimates the moment

magnitude M_W by about 0.5 magnitude units, but is otherwise approximately linearly

correlated with the latter (Figure 7d).

Site response

Based on the local geological conditions, the stations were divided into three groups,

depending on whether they are located on alluvial deposits, debris or colluvial deposits,

respectively rock. The geologic characteristics of the sites correspond to the following

approximate classification: soft soil, stiff soil and rock (Table 2). The GIT horizontal

Microsoft Office 1/16/11 10:06 PM

Deleted: In Figure 7a, the

Microsoft Office 1/15/11 6:09 PM

Deleted: -

Microsoft Office 1/16/11 10:07 PM

Deleted: ,

Microsoft Office 1/16/11 10:08 PM

Deleted: ese

1 component site response functions are shown in Figure 8 for six exemplary stations, with
2 two stations from each group. As mentioned earlier, station AND3 (not shown in Figure 7)
3
4 was chosen as the reference site, assuming a site response of unity, irrespective of
5
6 frequency, since this station is classified as a hard rock site and the H/V ratio is roughly flat
7
8 and approximately equal to one over the entire analyzed frequency band (Figure 4).
9

10
11 Figure 8 shows that in general, the obtained site response functions are well
12
13 constrained, with only small standard deviations resulting from the bootstrap analysis.
14
15 Overall, the rock sites show as expected lower values of the site response functions over the
16
17 entire frequency band than stiff and soft soil sites, with no evident predominant frequency
18
19 peaks. However, it can be clearly seen that also stations located on rock outcrops are not
20
21 completely devoid of amplification effects (e.g. station VDS3), which may be linked to the
22
23 weathered and fractured nature of the surface layers and to the shear-wave velocity gradient
24
25 (e.g. Theodulidis and Bard, 1995; Steidl et al., 1996). On the other hand, stations classified
26
27 as soft soil and stiff soil generally show more prominent amplification effects, with
28
29 amplification peaks at some given distinct frequencies (e.g. 4-5 Hz at station CLT3, 8 Hz at
30
31 station PGN3). The most significant amplification effects were obtained at station CMP3,
32
33 attaining a factor of about 14 at frequencies of about 8 and 12 Hz.
34

35
36 We also carried out a GIT inversion for the vertical (Z) component using the same S-
37
38 wave windows as chosen for the horizontal (H) one, and in order to corroborate the site
39
40 amplification functions obtained from the inversion, we calculated the H/V ratios directly
41
42 from the observed ground motion spectra as well. For the Z component GIT inversion, we
43
44 used the same reference condition as for the H component, i.e. the site response at station
45
46 AND3 is set to unity, irrespective of frequency.
47

Microsoft Office 1/16/11 10:09 PM

Deleted: a

Microsoft Office 1/16/11 10:09 PM

Deleted: ,

1
2 Figure 9 shows the comparison of the GIT H/Z ratio (i.e. the horizontal-to-vertical
3 ratio of the GIT site response functions, solid black line) and the H/V ratios (solid black
4 line with circles) [for the same six stations as depicted in Figure 8](#). The individual GIT site
5 amplification functions for the H (same as shown in Figure 8) and Z components are
6 indicated as well (grey lines with inverted triangles and squares, respectively). A first
7 observation is that the GIT H/Z ratio can satisfactorily explain the main features observed
8 in the H/V ratios (see for instance the peak at 4-5 Hz for station CLT3), with some
9 discrepancies only at low frequencies. These discrepancies may be linked to the fact that,
10 due to the reference condition, the GIT H/Z ratio at station AND3 is equal to unity, while at
11 the lowest frequencies, the H/V ratio observed at station AND3 starts to rise to about a
12 factor of two. Therefore, it is expectable that the GIT H/Z ratios slightly underestimate the
13 H/V ratios at low frequencies.
14
15

16
17
18
19
20
21
22
23
24
25
26 Another striking observation is given by the fact that the GIT site response function
27 of the Z component shows remarkable amplification effects for some stations (e.g. CMP3),
28 with the maximum of amplification shifted to higher frequencies as compared with the H
29 component. In such cases, the H/V ratio shows significant differences with the GIT H
30 amplification function, and as Parolai and Richwalski (2004) showed, this effect can be
31 linked [to S-P conversions at the bottom of the soft layer in the case of high-impedance](#)
32 contrasts, leading to a reduction of the H/V amplitude due to the amplification of the
33 vertical component at frequencies higher than the fundamental one. [Such high-frequency](#)
34 [amplification effects on the GIT Z component could also result if significant direct P-wave](#)
35 [energy is included in the chosen S-wave windows. This situation could occur if, by](#)
36 [selecting a time windows starting 1 sec before the S-wave onset, some late compressional](#)
37 [phases with significant amplitudes compared to the high-frequency S-wave part, or in the](#)
38
39
40
41
42
43
44
45
46
47
48
49

Microsoft Office 1/16/11 10:11 PM

Deleted: , for the same six stations as depicted in Figure 8,

Microsoft Office 1/16/11 10:19 PM

Deleted:

Microsoft Office 1/16/11 10:13 PM

Deleted: with

worst case at stations close to the considered source, the entire P-wave arrival were included the S-wave signal window. This effect is however not expected to be significant in our case, since the hypocentral distances are always larger than 5 km (which roughly corresponds to a minimum S-P travel time difference of 1 sec for typical upper crustal P-wave velocities), with most data points obtained at hypocentral distances of 10 km or larger. Furthermore, in the framework of the GIT methodology, the separation of source spectra and site response relies on a set of records sampling different distances for each earthquake and station. Finally, for stations showing only little amplification of the Z component (e.g. CLT3 or CSG3), the H/V ratio provides an acceptable first order approximation to the GIT H site response.

Microsoft Office 1/15/11 5:58 PM
Deleted: However, f

DISCUSSION AND CONCLUSIONS

Using the non-parametric GIT approach, we have investigated attenuation characteristics, source spectra, and site response functions for the ISNet seismic network, proving a means to better understand the influence of these different effects on ground motion amplitudes.

Microsoft Office 1/16/11 10:19 PM
Deleted: thus

We have determined non-parametric attenuation functions for 40 discrete frequencies between 1 and 30 Hz. These functions generally show a relatively simple shape, with a slight change in the rate of amplitude decay between 20 and 50 km. The quality factor Q based on the S-wave part of the recordings shows a pronounced frequency-dependence (close to linear), given by $Q(f) = 28.3f^{0.87}$. This S-wave attenuation model differs from the results of other authors reported for neighboring regions (Rovelli *et al.*, 1988; Malagnini *et al.*, 2000; Bianco *et al.*, 2002), and in particular shows a less severe frequency-dependence than the results derived by Castro *et al.* (2004b, 2008) for southern Italy. However, as stated above, it is important to keep in mind that the comparison of different models is

Microsoft Office 1/16/11 10:20 PM
Deleted: -

Microsoft Office 1/16/11 10:21 PM
Deleted:

1
2 complicated by the fact that the data used to estimate them sample different frequency
3
4 bands and different crustal volumes. Nevertheless, the differences in Q estimates over the
5
6 range of different studies and regions under investigation indicate that a significant lateral
7
8 variability in seismic attenuation characteristics exists in Italy. Indeed, Zolezzi et al. (2008),
9
10 performing an attenuation tomography study of the southern Apennines, showed for
11
12 instance that the attenuation structure clearly differs on the Tyrrhenian side with respect to
13
14 the Adriatic side of the southern Apennines chain.

15
16 The earthquake spectra corrected for attenuation were used to derive source
17
18 parameters following the ω^2 -model (Brune, 1970, 1971), since the inverted source spectra
19
20 can be well explained with the ω^2 spectral shape. The obtained corner frequencies and
21
22 seismic moments provide indications that at least in the narrow magnitude range under
23
24 investigation, self-similar scaling seems to hold almost perfectly. However, we
25
26 acknowledge that of course the magnitude range $M_L=1.5-3.1$ is by far too small to speculate
27
28 upon any general scaling characteristics of earthquakes in the region. The stress drops range
29
30 from 0.01 to about 2 MPa, which is close to the lower bounds typically observed for crustal
31
32 earthquakes (0.1-100 MPa, e.g. Kanamori, 1994). Thus, the earthquakes under investigation
33
34 in this study seem to show only rather weak high-frequency energy radiation. This
35
36 conclusion is also compatible with the observation that the local magnitude M_L seems to
37
38 systematically underestimate M_W by about 0.5 magnitude units.

39
40 Finally, the results of the spectral inversion and the H/V analysis point out that only
41
42 few stations of [the ISNet network](#) are not noticeably affected by site effects. Such stations
43
44 are, as expected, located on rock sites. In addition, some stations located on what appears to
45
46 be competent rock show amplification in the high frequency range. This could be explained
47
48 by taking into account the effect of a near-surface, low-velocity layer due to the presence of
49

1 weathered rock, but also topographic effects might play a role. However, the unfortunately
2 rather poor knowledge of the geologic units below the stations does not allow for any
3
4
5
6 definitive conclusion, and in order to better understand how the observed amplification
7
8 effects are caused in detail, geotechnical information of subsurface structure is required.
9

10 As we have shown, the maximum amplification is generally shifted to higher
11 frequencies in the Z component as compared with the H component, and in some cases,
12 significant amplification effects are visible on the Z component. In such cases, S-P
13 conversions at the bottom of the soft layer could explain the simultaneously observed
14 reduction of the H/V amplitude due to this amplification on the Z component at frequencies
15 higher than the fundamental one, causing an increased disagreement between the GIT H
16 site response and H/V ratio function. Summarizing our site response results, we can hence
17 state that our observations are in good agreement with previous studies, in particular also
18 with respect to the comparison of GIT and H/V site response estimates (e.g., Field and
19 Jacob, 1995; Bonilla et al., 1997; Parolai et al., 2004), which have shown that the H/V
20 method provides a good estimate of the fundamental frequency of resonance of S-waves,
21 but often underestimates the level of amplification with respect to the GIT approach.
22
23
24
25
26
27
28
29
30
31
32

33
34 On the basis of our findings, we finally conclude that the results presented in this
35 study allow for an improved characterization of the seismic recordings obtained by the
36 ISNet network. This characterization is of particular importance since the data streams
37 recorded by the ISNet network are intended for usage in real-time seismic information
38 systems (i.e., early warning and near real-time shake map estimation, Iannacone et al.,
39 2010), and our results provide a means to incorporate knowledge of the attenuation
40 structure, site effects modifying ground motions at the ISNet stations as well as potential
41 correction factors in magnitude estimation into these systems.
42
43
44
45
46
47
48
49
50
51
52
53
54
55
56
57
58
59
60
61
62
63
64
65

Micro Soft 1/18/11 3:55 PM
Deleted: provide useful information for the seismic early warning system and the near real-time estimation of shake maps for rapid emergency management in the in Irpinia-Basilicata region by

Micro Soft 1/18/11 3:55 PM
Deleted: ing

Micro Soft 1/18/11 3:55 PM
Deleted: and

ACKNOWLEDGMENTS

The data used in this study were recorded by ISNet (Irpinia Seismic Network) managed by Amra Scarl (Analisi e Monitoraggio del Rischio Ambientale) and are available online through <http://isnet.na.infn.it/>. Data availability is subject to registration. Some of the figures were drawn with the software Generic Mapping Tools (www.soest.hawaii.edu/gmt). This work was performed during a three months visit of L. Cantore at the GFZ German Research Centre for Geosciences in Potsdam, Germany, in the framework of a DAAD (Deutscher Akademischer Austausch Dienst) grant. We would like to thank Marco Mucciarelli and an anonymous reviewer for constructive comments that helped to improve the manuscript.

REFERENCES

- Anderson, J. and S. Hough (1984). A model for the shape of the Fourier amplitude spectrum of acceleration at high frequencies. Bull Seism. Soc. Am. 74, 1969-1993.
- Andrews, D. J. (1986). Objective determination of source parameters and similarity of earthquakes of different size. Geophysical Monographs 37, 6, 259-267.
- Archuleta, R. J., and J. H. Steidl (1998). ESG studies in the United States: results from borehole arrays in The Effects of Surface Geology on Seismic Motion, K. Irikura, K. Kudo, H. Okada, and T. Sasatani (editors) Vol. 1, Balkema, Rotterdam, 3-14.
- Beresnev, I. A. (2001). What we can and cannot learn about earthquake sources from the spectra of seismic waves. Bull. Seismol. Soc. Am. 91, 397-400.
- Beresnev, I. A. (2002). Source parameters observable from the corner frequency of earthquake spectra. Bull. Seismol. Soc. Am. 92, 2047-2048.
- Bianco, F., E. Del Pezzo, M. Castellano, J. Ibanez, and F. Di Luccio (2002). Separation of

Micro Soft 1/18/11 3:56 PM

Deleted: Page Break

Microsoft Office 1/15/11 6:11 PM

Deleted: ... (1)

Micro Soft 1/19/11 2:33 PM

Deleted: The data used in this study were recorded by ISNet (Irpinia Seismic Network) managed by Amra Scarl (Analisi e Monitoraggio del Rischio Ambientale) and are available online at <http://dbserver.ov.ingv.it:8080>.

Microsoft Office 1/16/11 10:25 PM

Deleted: Page Break

Microsoft Office 1/15/11 6:12 PM

Deleted: BAKLEMA

1
2 intrinsic and scattering seismic attenuation in the Southern Apennine zone, Italy.
3
4 Geophys. J. Int. 150 10–22.

5
6 Bernard, P., and A. Zollo (1989). The Irpinia (Italy) 1980 earthquake: Detailed analysis of a
7
8 complex normal faulting, J. Geophys. Res. B94, 1631–1647.
9

10
11 Bonilla, L. F., J. H. Steidl, G. T. Lindley, A. G. Tumarkin, and R. J. Archuleta (1997). Site
12
13 amplification in the San Fernando Valley, California: variability of site-effect
14
15 estimation using the S-wave, coda and H/V methods. Bull. Seismol. Soc. Am. 87,
16
17 710–730.

18
19 Brune, J. N. (1970). Tectonic stress and the spectra of seismic shear waves from
20
21 earthquakes. J. Geophys. Res. 75, 4997-5009.

22
23 Brune, J.N. (1971). Correction. J. Geophys. Res. 76, 5002.

24
25 Castro, R. R., J. G. Anderson, and S. K. Singh (1990). Site response, attenuation and source
26
27 spectra of S waves along the Guerrero, Mexico, subduction zone. Bull. Seismol. Soc.
28
29 Am. 80, 1481–1503.

30
31
32 Castro, R. R., F. Pacor, D. Bindi, G. Franceschina and L. Luzi (2004a): Site response of
33
34 strong motion stations in the Umbria, Central Italy, Region. Bull. Seismol. Soc. Am.
35
36 **94** (2), 576-590.

37
38 Castro, R. R., M.R. Gallipoli and M. Mucciarelli (2004b): An attenuation study in
39
40 Southern Italy using local and regional earthquakes recorded by seismic network of
41
42 Basilicata. Annals of Geophys. **47**(5), 1597-1608.

43
44 [Castro, R.R., M.R. Gallipoli, and M. Mucciarelli \(2008\). Crustal Q in Southern Italy](#)
45
46 [determined from regional earthquakes. Tectonophysics 457, 96-101.](#)

47
48 Cinti, F. R., L. Faenza, W. Marzocchi, and P. Montone (2004). Probability map of the next
49

1 M \geq 5.5 earthquakes in Italy. *Geochemistry, Geophysics, Geosystem*, 5, Q 11003,
2
3
4 doi: 10.1029/2004GC000724.

5
6 Convertito, V., R. De Matteis, L. Cantore, A. Zollo and G. Iannaccone (2009). Rapid
7
8 estimation of ground-shaking maps for seismic emergency management in the
9
10 Campania region of Southern Italy. *Natural Hazards*, doi: 10.1007/s11069-009-9359-
11
12 2.

13
14 Efron, B., and R. J. Tibshirani (1994). *An Introduction to the Bootstrap*. Chapman and Hall,
15
16 London.

17
18 Emolo, A., G. Iannaccone, A. Zollo, and A. Gorini (2004). Inferences on the source
19
20 mechanisms of the 1930 Irpinia (southern Italy) earthquake from simulations of the
21
22 kinematic rupture process. *Ann. Geophys.* 47, 1743–1754.

23
24 Field, E. H., and K. H. Jacob (1995). A comparison and test of various site-response
25
26 estimation techniques, including three that are not reference-site dependent. *Bull.*
27
28 *Seism. Soc. Am.* 4, 1127-1143.

29
30 Hanks, T. C., and H. Kanamori (1979). A moment magnitude scale, *J. Geophys. Res.* 84,
31
32 2348–2350.

33
34 Hanks, T.C., and Thatcher, W. (1972). A graphical representation of seismic source
35
36 parameters. *J. Geophys. Res.*, 77(23), 4393-4405.

37
38 [Iannaccone, G., Zollo, A., Elia, L., Convertito, V., Satriano, C., Martino, C., Festa, G.,
39
40 Lancieri, M., Bobbio, A., Stabile, T., Vassallo, M., and Emolo, A. \(2010\). A
41
42 prototype system for earthquake early-warning and alert management in southern
43
44 Italy. *Bull. Earthq. Eng.*, 8, 1105-1129, doi:10.1007/s10518-009-9131-8.](#)

45
46
47
48 [Kanamori, H. \(1994\). Mechanics of earthquakes, *Ann. Rev. Earth Planet. Sci.* 22, 207–237.](#)

Micro Soft 1/18/11 3:57 PM

Formatted: Font:(Default) Times New Roman

Micro Soft 1/18/11 3:57 PM

Formatted: Justified, Indent: Left: 0 cm, Hanging: 1 cm, Space After: 6 pt, Line spacing: double

Micro Soft 1/18/11 3:57 PM

Formatted: Font:(Default) Times New Roman

Micro Soft 1/18/11 3:57 PM

Formatted: Font:(Default) Times New Roman, Not Italic

Micro Soft 1/18/11 3:57 PM

Formatted: Font:(Default) Times New Roman

Micro Soft 1/18/11 3:57 PM

Deleted: .

1
2 Konno, K., and T. Ohmachi (1998). Ground-motion characteristics estimated from spectral
3
4 ratio between horizontal and vertical components of microtremor. *Bull. Seismol. Soc.*
5
6 *Am.* 88, 228–241.
7
8 Langston, C. A. (1979). Structure under Mount Rainier, Washington, inferred from
9
10 teleseismic body waves. *J. Geophys. Res.* 84, 4749-4762.
11
12 Lermo, J., and F. J. Chavez-Garcia (1993). Site effect evaluation using spectral ratios with
13
14 only one station. *Bull. Seism. Soc. Am.* 83, 1574-1594.
15
16 Malagnini, L., R. B. Herrmann and M. Di Bona (2000). Ground-motion scaling in the
17
18 Apennines (Italy). *Bull. Seismol. Soc. Am.*, **90** (4), 1062-1081.
19
20
21 Menke, W. (1989). *Geophysical Data Analysis: Discrete Inverse Theory*, International
22
23 *Geophysics Series*, Academic Press, New York.
24
25
26 Montone, P., M. T. Mariucci, S. Pondrelli, and A. Amato, (2004). An improved stress map
27
28 for Italy surrounding regions (central Mediterranean). *J. Geophys. Res.* 109, B10410,
29
30 doi: 10.1029/2003JB002703.
31
32 Nakamura, Y. (1989). A method for dynamic characteristics estimations of subsurface
33
34 using microtremors on the ground surface. *Q. Rep. Railway Tech. Res. Inst. Japan*,
35
36 30, 25-33.
37
38 Oth, A., D. Bindi, S. Parolai, and F. Wenzel (2008). S-wave attenuation characteristics
39
40 beneath the Vrancea region in Romania: new insights from the inversion of ground-
41
42 motion spectra. *Bull. Seismol. Soc. Am.* 98, no. 5, 2482–2497, doi:
43
44 10.1785/0120080106.
45
46
47
48
49
50
51
52
53
54
55
56
57
58
59
60
61
62
63
64
65

1
2 Oth, A., Parolai, S., Bindi, D., and Wenzel, F. (2009). Source spectra and site response
3
4 from S waves of intermediate-depth Vrancea, Romania, earthquakes. *Bull. Seismol.*
5
6 *Soc. Am.* 99, 235-254, doi: 10.1785/0120080059.
7
8 Pantosti, D., and G. Valensise (1990). Faulting mechanism and complexity of the 23
9
10 November 1980, Campania-Lucania earthquake, inferred from surface observations.
11
12 *J. Geophys. Res.* 95, 15319–15341.
13
14 Parolai, S., D. Bindi, and P. Augliera (2000). Application of the generalized inversion
15
16 technique (GIT) to a microzonation study: numerical simulations and comparison
17
18 with different site-estimation techniques. *Bull. Seismol. Soc. Am.* 90, 286–297.
19
20 Parolai, S., and S. M. Richwalski (2004). The importance of converted waves in comparing
21
22 H/V and RSM site response estimates. *Bull. Seismol. Soc. Am.* 94, 304–313.
23
24 Parolai, S., D. Bindi, M. Baumbach, H. Grosser, C. Milkereit, S. Karakisa, and S. Zünbül
25
26 (2004). Comparison of different site response estimation techniques using aftershocks
27
28 of the 1999 Izmit earthquake. *Bull. Seismol. Soc. Am.* 94, 1096–1108.
29
30
31 Rovelli, A., O. Bonamassa, M. Cocco, M. Di Bona and S. Mazza (1988). Scaling laws and
32
33 spectral parameters of the ground motion in active extensional areas in Italy. *Bull.*
34
35 *Seismol. Soc. Am.*, 78 (2), 530-560.
36
37 Steidl, J., A. G. Tumarkin, and R. J. Archuleta (1996). What is a reference site? *Bull.*
38
39 *Seism. Soc. Am.* 86, 1733-1748.
40
41 Theodulidis, N. and Bard, P.-Y. (1995). Horizontal to vertical spectral ratio and geological
42
43 conditions: an analysis of strong motion data from Greece and Taiwan. *Soil. Dyn.*
44
45 *Earthquake Eng.*, 14,177–197.
46
47
48
49

1
2
3
4
5
6
7
8
9
10
11
12
13
14
15
16
17
18
19
20
21
22
23
24
25
26
27
28
29
30
31
32
33
34
35
36
37
38
39
40
41
42
43
44
45
46
47
48
49
50
51
52
53
54
55
56
57
58
59
60
61
62
63
64
65

Weber, E., V. Convertito, G. Iannaccone, A. Zollo, A. Bobbio, L. Cantore, M. Corciulo, M. Di Crosta, L. Elia, C. Martino, A. Romeo, and C. Satriano (2007). An advanced seismic network in the southern Apennines (Italy) for seismicity investigations and experimentation with earthquake early warning. *Seism. Res. Lett.* 78, 622–534.

Westaway, R. (1987). The Campania, southern Italy, earthquakes of 1962 August 21. *Geophys. J. R. Astr. Soc.* 8, 1–24.

Westaway, R., and J. Jackson (1987). The earthquake of 1980 November 23 in Campania-Basilicata (southern Italy). *Geophys. J. R. Astr. Soc.* 90, 375–443.

Zolezzi, F., P. Morasca, K. Mayeda, W. S. Phillips, and C. Eva (2008). Attenuation tomography of the Southern Apennines (Italy). *J. Seismol.* 12, 355–365.

1
2
3
4
5
6
7
8
9
10
11
12
13
14
15
16
17
18
19
20
21
22
23
24
25
26
27
28
29
30
31
32
33
34
35
36
37
38
39
40
41
42
43
44
45
46
47
48
49
50
51
52
53
54
55
56
57
58
59
60
61
62
63
64
65

TABLES

Table 1: S-wave attenuation models reported for Italy

Region	Frequency range (Hz)	Q-model	Geometrical spreading	Reference
Central and Central-southern Apennines	$0.1 \leq f \leq 20$	$Q(f) = 100 f$	$1/r$	Rovelli et al. (1988)
Entire Apennines	$0.24 \leq f \leq 5.0$	$Q(f) = 130 f^{0.1}$	$r^{-0.9}, r \leq 30$ km $r^0, 30 \leq r \leq 80$ km $r^{-0.5}, r \geq 80$ km	Malagnini et al. (2000)
Umbria-Marche	$0.3 \leq f \leq 9.5$	$Q(f) = 31.2 f^{1.2}$	$1/r$	Castro et al. (2004a)
Southern Italy	$1.6 \leq f \leq 10$	$Q(f) = 32.1 f^{1.7}$	$10/r^b$ $b=1.0 \pm 0.2$	Castro et al. (2004b)
Irpinia-Basilicata (southern Italy)	$1 \leq f \leq 30$	$Q(f) = 27.1 f^{0.95}$	$5/r$ (reference distance 5 km)	This study

Table 2: List of stations with the respective geological underground classification

CGG3	stiff soil
LIO3	stiff soil
CMP3	stiff soil
TEO3	stiff soil
CLT3	soft soil
RDM3	stiff soil
COL3	stiff soil
SCL3	stiff soil
CSG3	rock
PST3	stiff soil
SNR3	rock
AND3	rock
VDP3	stiff soil
STN3	rock
NSC3	rock
PGN3	stiff soil
SRN3	soft soil
VDS3	rock
BEL3	soft soil
RSF3	stiff soil
AVG3	rock
MNT3	stiff soil

1
2
3
4
5
6
7
8
9
10
11
12
13
14
15
16
17
18
19
20
21
22
23
24
25
26
27
28
29
30
31
32
33
34
35
36
37
38
39
40
41
42
43
44
45
46
47
48
49
50
51
52
53
54
55
56
57
58
59
60
61
62
63
64
65

FIGURE CAPTIONS

Figure 1. Stations of the ISNet seismic network used in this work. Grey circles indicate rock, black triangles stiff soil and open squares soft soil sites (see also Table 2). The solid black lines represent the surface projection of the three fault segments that ruptured during the 23 November 1980 earthquake (M 6.9).

Figure 2. Station locations (triangles), traces of fault segments (solid black lines), and source-station paths (grey lines) of the considered dataset. Two cross-sections through the epicentral area (one with latitude, one with longitude) are depicted as well.

Figure 3. a) Local magnitude M_L versus hypocentral distance R distribution for the dataset used in the inversion. b) Number of events with given M_L for the dataset used in the inversion.

Figure 4. Average H/V ratio calculated at station AND3. The grey-shaded area indicates the standard deviation. Note the approximately flat shape, with a slight rise above a value of 2 only at low frequencies.

Figure 5. a) Non-parametric attenuation functions (distance range 5-83 km) at 40 frequencies (1-30 Hz) obtained in the first step of the inversion scheme. The functions are color-coded with respect to the corresponding frequency (see legend). b) Two of the attenuation functions depicted in a) with their respective standard deviation from bootstrap analysis indicated as grey-shaded areas.

Figure 6. $Q(f)$ model derived from the analysis of the non-parametric attenuation functions shown in Figure 5 (solid black line). Dots and error bars indicate the individual Q -values obtained at each considered frequency, and the solid black line represents the fit to these data points of the form $Q(f)=Q_0f^N$. Other models from the literature are indicated in their

1 frequency range of validity (overlapping with our frequency range) for comparison (see
2 text).
3
4

5
6 **Figure 7.** Source results obtained from the spectral inversion. a) All source spectra (in
7 acceleration) as derived from the GIT inversion at a reference distance of $R_0=5$ km, color-
8 coded with respect to their M_L values. Green dashed lines indicate ω^2 model fits. b) Corner
9 frequency versus seismic moment plot. The grey line indicates a log-linear fit, with a slope
10 close to the expected theoretical value of $-1/3$ in the case of self-similar scaling. c) Stress
11 drop values computed as given in equation (6). d) Local magnitude M_L versus moment
12 magnitude M_W as estimated from the spectral fits shown in a). Note that M_L systematically
13 underestimates M_W by about 0.5 magnitude units.
14
15
16
17
18
19
20
21

22 **Figure 8.** Calculated GIT site response functions for six stations. The solid line indicates
23 the mean with the grey-shaded area depicting the standard deviation of 200 bootstrap
24 samples. The top panels are examples for stations classified as rock sites (see Table 2),
25 while the middle and bottom panels relate to stations classified as stiff and soft soil,
26 respectively.
27
28
29
30
31

32 **Figure 9.** Comparison of H/V ratios calculated directly from the ground motion spectra
33 (black lines with circles) and the GIT H/Z ratios (i.e. GIT site response on H component
34 divided by GIT site response on Z, black solid lines) for the same six stations as depicted in
35 Figure 8. The individual GIT site response functions for horizontal and vertical component
36 are indicated as well with grey lines with inverse triangles and squares, respectively.
37
38
39
40
41
42
43
44
45
46
47
48
49
50
51
52
53
54
55
56
57
58
59
60
61
62
63
64
65

FIGURES

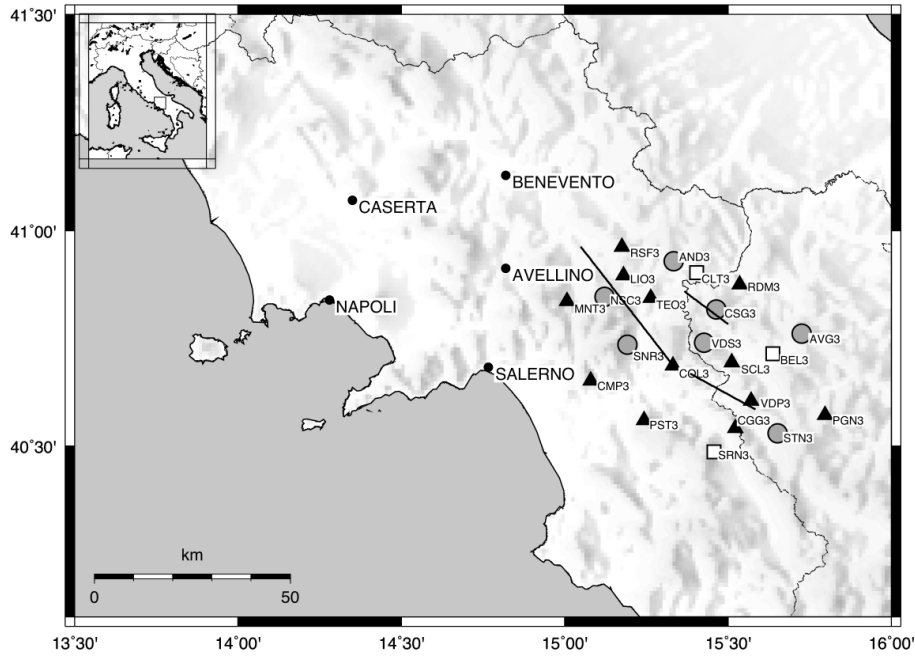


Figure 1

1
2
3
4
5
6
7
8
9
10
11
12
13
14
15
16
17
18
19
20
21
22
23
24
25
26
27
28
29
30
31
32
33
34
35
36
37
38
39
40
41
42
43
44
45
46
47
48
49
50
51
52
53
54
55
56
57
58
59
60
61
62
63
64
65

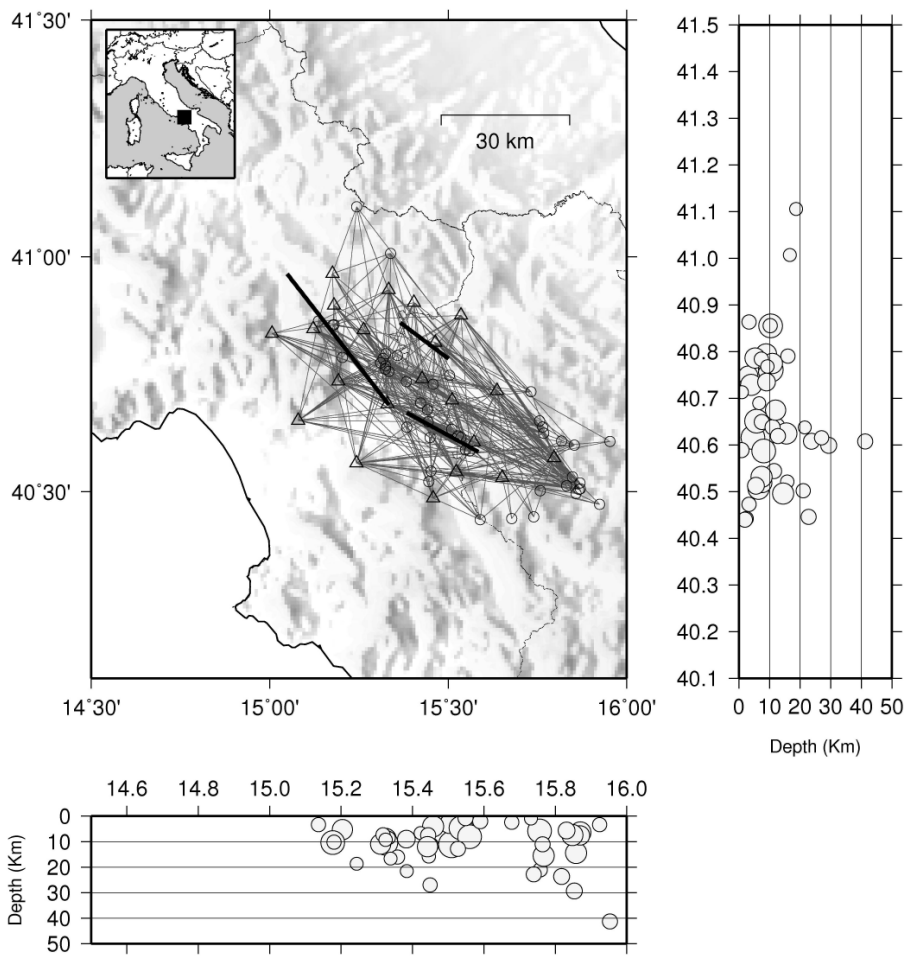


Figure 2

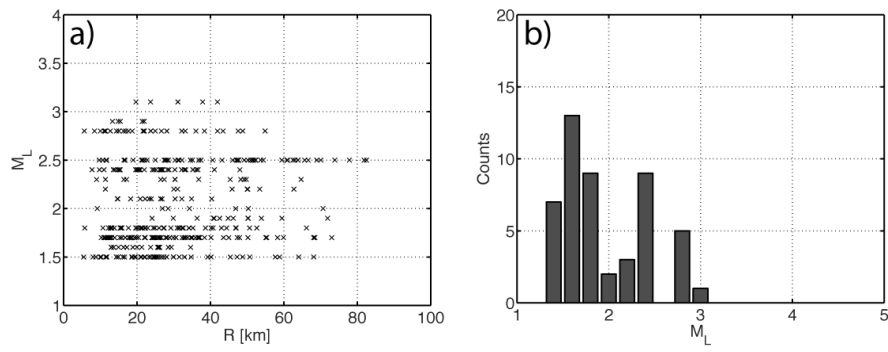


Figure 3

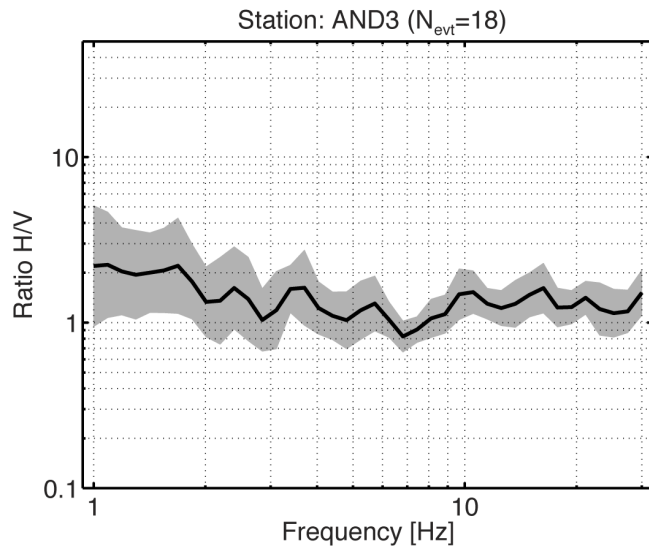


Figure 4

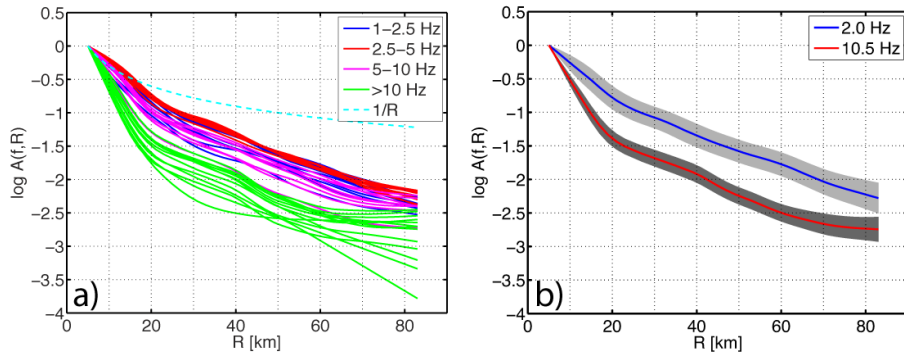


Figure 5

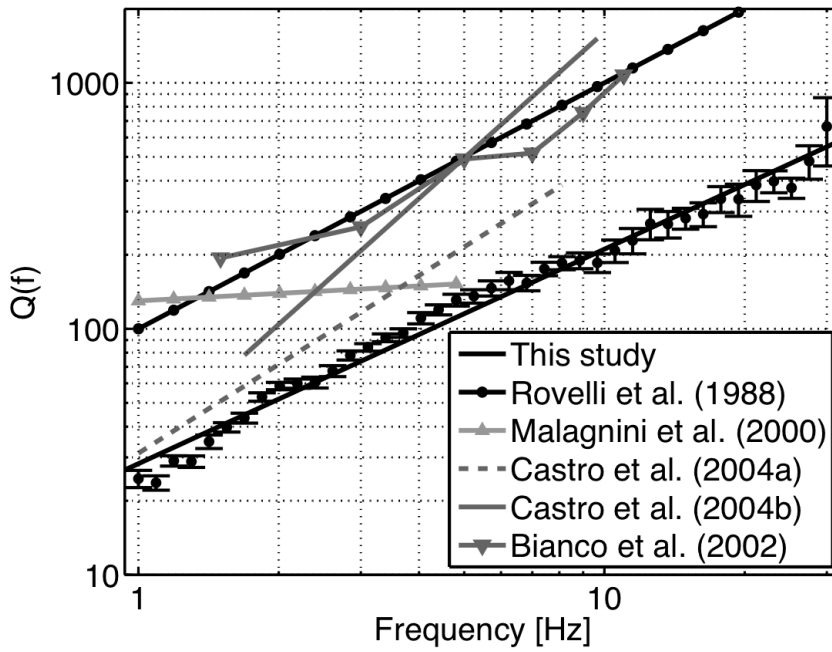


Figure 6

1
2
3
4
5
6
7
8
9
10
11
12
13
14
15
16
17
18
19
20
21
22
23
24
25
26
27
28
29
30
31
32
33
34
35
36
37
38
39
40
41
42
43
44
45
46
47
48
49
50
51
52
53
54
55
56
57
58
59
60
61
62
63
64
65

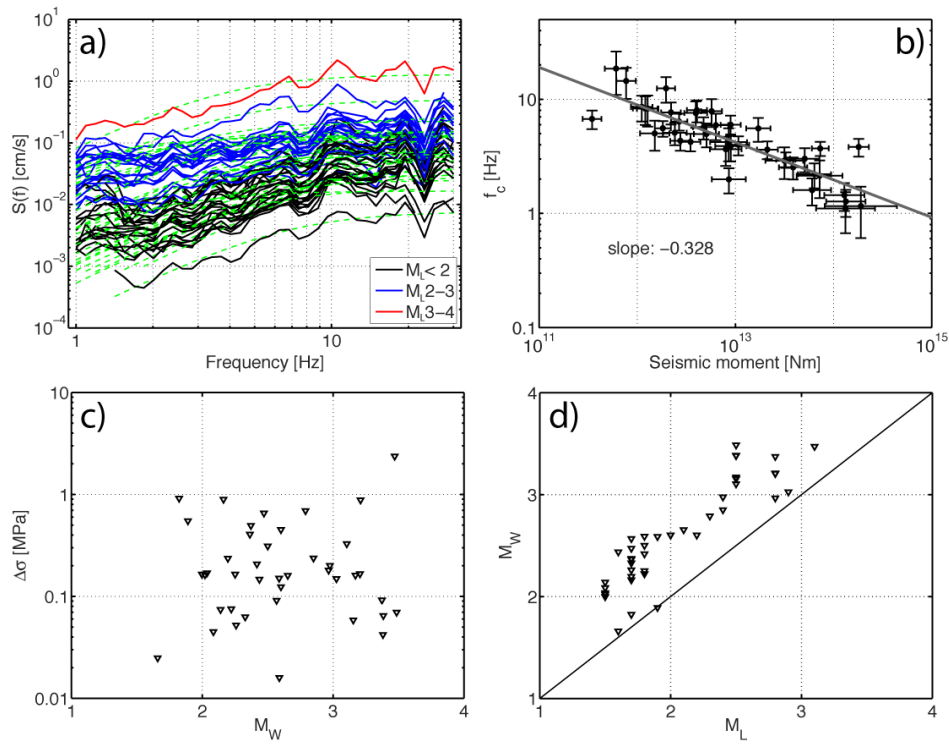


Figure 7

1
2
3
4
5
6
7
8
9
10
11
12
13
14
15
16
17
18
19
20
21
22
23
24
25
26
27
28
29
30
31
32
33
34
35
36
37
38
39
40
41
42
43
44
45
46
47
48
49
50
51
52
53
54
55
56
57
58
59
60
61
62
63
64
65

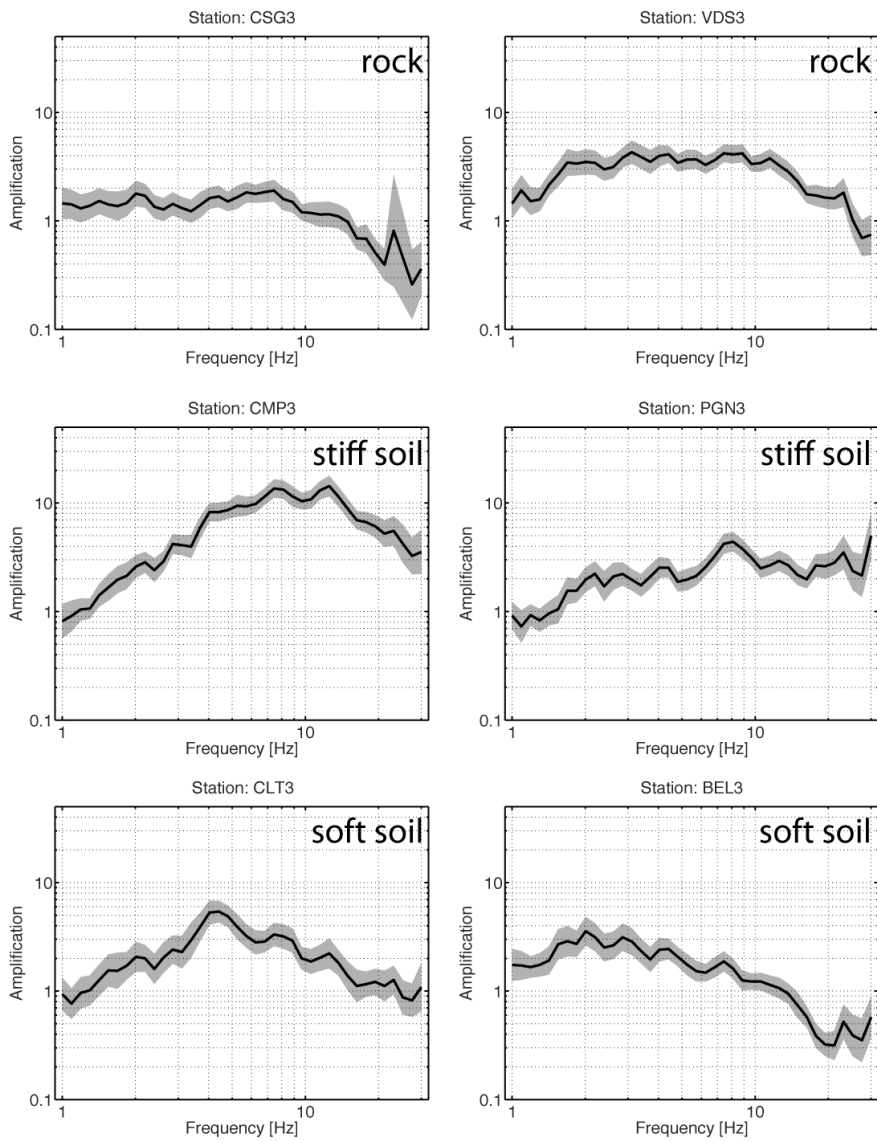


Figure 8

1
2
3
4
5
6
7
8
9
10
11
12
13
14
15
16
17
18
19
20
21
22
23
24
25
26
27
28
29
30
31
32
33
34
35
36
37
38
39
40
41
42
43
44
45
46
47
48
49
50
51
52
53
54
55
56
57
58
59
60
61
62
63
64
65

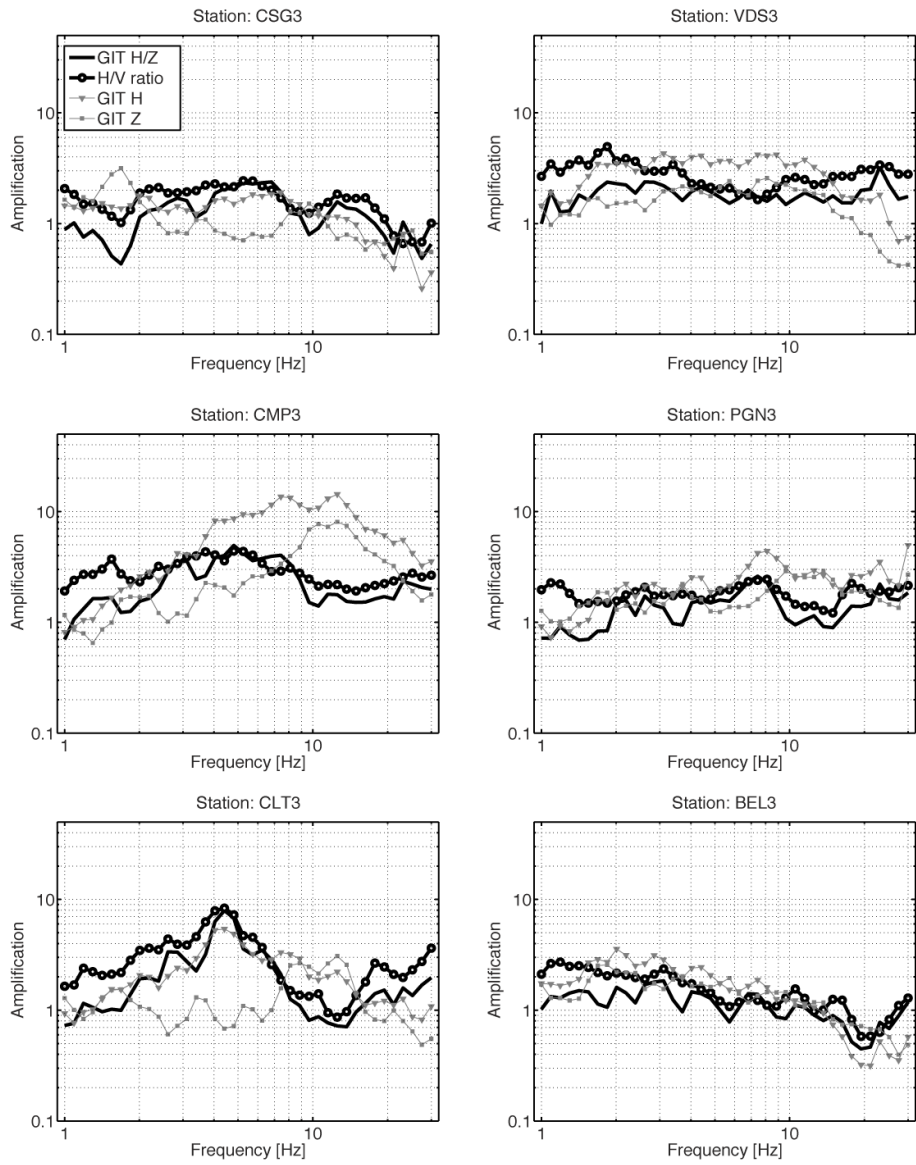


Figure 9